[redacted]

NASA TM X-1081

EFFECTS OF A STING SUPPORT ON THE SUPERSONIC FORCE AND MOMENT CHARACTERISTICS OF AN APOLLO MODEL AT ANGLES FROM -30° TO +185°

By Louis S. Stivers, Jr.

Ames Research Center
Moffett Field, Calif.

[redacted]

NATIONAL AERONAUTICS AND SPACE ADMINISTRATION

[redacted]

[redacted]

EFFECTS OF A STING SUPPORT ON THE SUPERSONIC FORCE AND MOMENT CHARACTERISTICS OF AN APOLLO MODEL AT ANGLES FROM -30° TO +185°*

By Louis S. Stivers, Jr.

Ames Research Center
Moffett Field, Calif.

SUMMARY

Force and moment characteristics of an early configuration of the Apollo Command Module were measured in a wind tunnel at Mach numbers of 5.45 and 3.29, with corresponding Reynolds numbers of 0.68 million and 1.07 million, respectively. Several models having different mounting attitudes were used to obtain data at angles of attack from -30° to +185° with the sting inclined through a range of angles no greater than ±30°, relative to the free-stream direction. Also included in the investigation were brief tests at a Mach number of 3.29 to determine the effects of changing Reynolds number from 0.28 million to 1.07 million and to determine some of the characteristics of the flow on the surface of the models.

Effects of sting-support inclination were significant only for the pitching-moment coefficients and were observed for a Mach number of 5.45 and a Reynolds number of 0.68 million even when the inclinations of the sting were limited to ±10°. The results for the two Reynolds numbers for a Mach number of 3.29 indicated that the effects of sting inclination might be less at higher Reynolds numbers. The pitching-moment coefficients for a Mach number of 5.45 associated with two particular combinations of model mounting angle and sting-support inclination, which corresponded to angles of attack very near the aerodynamic trim points, were judged to be essentially unaffected by sting inclination. An attempt was also made to determine whether the data were influenced by the length and the diameter of the sting.

In general, force and moment characteristics were predicted fairly well by modified Newtonian theory. The effects of angle of attack on the location of the stagnation point and on the regions of separation determined from a surface-flow study are presented in graphical form. The location of the stagnation point on the large spherical portion (heat-shield face) of the Apollo Command Module, as affected by angle of attack, was predicted reasonably well by an empirical method.

---

*Title, Unclassified

[redacted]

INTRODUCTION

A large amount of the aerodynamic data required for the design of the Apollo Spacecraft System has been obtained from wind-tunnel tests of models of the component parts which make up the system. For such tests the models were generally mounted on some kind of sting-support arrangement. Furthermore, in some of the tests the sting supports were inclined to high incidences relative to the free-stream direction so that data could be acquired for the wide range of angles of attack. It is well known that before wind-tunnel data can be utilized with confidence, support-interference effects must be considered.

A representative selection of the presently available sting-interference data, obtained for a wide range of Mach numbers from subsonic to hypersonic values, is given in references 1 to 7. Most of these data, however, are strictly applicable only to slender bodies and cannot be expected to be appropriate for tests of a sting-supported short, blunt body like the Apollo Command Module. This follows because of the marked differences in the characteristics of the afterbody flow for these two body types, especially for high supersonic Mach numbers (e.g., see ref. 8). Of the known published data only those of reference 7 apply strictly to a blunt body, and then only for a Mach number of about 19 and for incidences of the sting support near 0°. It is believed, however, that certain basic knowledge from past investigations of wake flow and sting interference should prove valuable in an appraisal of some of the effects of a sting employed during the tests of a blunt body.

The purposes of this report are to present the force and moment characteristics of an early configuration of the Apollo Command Module for Mach numbers of 5.45 and 3.29 and to provide information concerning the effects of sting-support inclination on these force and moment data. Also, this report presents selected basic information, from sting-interference and related wake-flow studies, which suggest a criterion for the selection of a length of sting behind any type body such that no appreciable interference will be introduced to the flow over the body by the structure supporting the sting. The force and moment data for the Apollo Command Module were obtained from wind-tunnel tests for angles of attack from -30° to $+185^\circ$ with the sting support inclined through a range of incidences from -30° to $+30^\circ$, measured relative to the free-stream direction.

NOTATION

C_A total axial-force coefficient, $\dfrac{\text{total measured axial force}}{q_\infty S}$

C_D total drag coefficient, $\dfrac{\text{total drag}}{q_\infty S}$

C_L lift coefficient, $\dfrac{\text{lift}}{q_\infty S}$

C_m pitching-moment coefficient about moment center (see fig. 1), $\frac{\text{pitching moment}}{q_\infty Sd}$

$C_{m_{axis}}$ pitching-moment coefficient about a point on the axis of revolution of the model (see fig. 1)

C_N normal-force coefficient, $\frac{\text{normal force}}{q_\infty S}$

C_{p_b} balance-cavity pressure coefficient, $\frac{p_b - p_\infty}{q_\infty}$

d model maximum diameter

d_s shroud diameter of sting-supported force and moment balance

i_α model mount offset angle in the pitch plane, measured from model apex-forward attitude, deg

$\frac{L}{D}$ lift-drag ratio, $\frac{C_L}{C_D}$

M Mach number

p_b static pressure in balance cavity of model

p_∞ free-stream static pressure

q_∞ free-stream dynamic pressure

R Reynolds number

r radial distance measured from axis of symmetry of body

r_{max} maximum radius measured from axis of symmetry of body, $\frac{d}{2}$

S reference area of model, $\frac{\pi}{4} d^2$

x longitudinal distance from moment center to large spherical surface (heat shield) (see fig. 1)

x_{cp} longitudinal distance from center of pressure to large spherical surface

z vertical distance from moment center to axis of symmetry (see fig. 1)

α angle of attack measured from model apex-forward attitude, deg

α_s inclination of the sting relative to the free-stream direction, deg

θ azimuthal angle about axis of symmetry of body measured from meridian plane, viewed from the large spherical surface (heat shield) toward the apex of the conical portion of the body

APPARATUS AND TEST INFORMATION

Test Facility

The tests were conducted in the Ames 1- by 3-Foot Supersonic Wind Tunnel, which is a closed-circuit, continuous-operation tunnel. A flexible nozzle and the capacity for varying stagnation pressure up to 59 psia permit operation of the tunnel from a Mach number of about 1.4 to 6, at maximum Reynolds numbers of approximately 0.2 to 0.7 million per inch, depending on the Mach number.

Models and Equipment

Models of an early configuration of the Apollo Command Module (fig. 1) were tested. Nine models constructed by North American Aviation, Inc., were loaned to the Ames Research Center for the present tests. The models, illustrated in figure 2(a), are 0.02 scale (3.08 in. in diameter) and are identical except for the different angular offsets of the balance cavity. The offsets, which are in the pitch plane, permit the model to be mounted at attitudes from 0° to 140° in 20° increments, and at 180°. This arrangement coupled with a variable-angle sting support allows the model to be tested at angles of attack from -30° to $+185^\circ$ with substantial overlapping of the angles, yet without exceeding sting inclinations of $\pm 30^\circ$. Two other models, constructed at the Ames Research Center, are illustrated in figure 2(b). These two models are 3 inches in diameter and have angular offsets of 140° and 180°.

The models were inverted on a sting-supported strain-gage balance. Figure 3 shows the 0° offset model ready for testing. Because of different balance-cavity diameters in the two sets of models, different balances were used. Each balance was shielded from the air stream by a shroud which had a diameter 0.28 of the model diameter. The combined shroud and sting extended downstream of the model with no significant change in diameter for a distance of about 3 model diameters (see fig. 3). At this location the sting bent through an angle of 45° in the pitch plane and extended downstream an additional model diameter before turning laterally to the tunnel wall. The lateral length of the sting support system was housed within a double-wedge-section fairing which was maintained in approximate alinement with the stream direction during changes in sting incidence. The model and sting-support assembly rotated in pitch about an axis located about one-half model diameter downstream of the model base.

Pressures in the balance cavity were measured during most of the tests with a differential-type pressure transducer. With this transducer differential pressures up to 0.34 lb/sq in. could be measured to an accuracy of ±0.001 lb/sq in.

Tests

Normal force, axial force, pitching moment, and balance-cavity pressure were measured for each of the nine 3.08-inch-diameter models during tests at a Mach number of 5.45. The sting support was inclined from -30° to $+30^{\circ}$ in 5° increments for each model except for the one with 180° offset. This provided a 40° angle-of-attack overlap of the data between these models. A check showed that the measured data for the 140° offset model were invalid, except for the balance-cavity pressures. Furthermore, supersonic flow in the tunnel was difficult to maintain with the models offset 140° and 180°. For the 180° offset model, supersonic flow could be maintained only for three sting-support incidences. Accordingly, the data for these two models were supplemented by corresponding data from tests of the two 3-inch-diameter models which had 5 percent less cross-sectional area than the larger models. No difficulty was experienced in maintaining the flow at a Mach number of 5.45 during the tests of these smaller models. Both sets of the above models were tested at a Reynolds number of 0.68 million, based on the model diameter.

Limited tests also were conducted at a Mach number of 3.29 and Reynolds number of 1.07 million in which force and moment data were measured for the 3.08-inch-diameter 60° and 80° offset models, and for the 3-inch-diameter 140° and 180° offset models. In addition, the tests of the 3-inch-diameter models at a Mach number of 3.29 were repeated at a reduced Reynolds number of 0.28 million.

Balance-cavity pressures were measured only for the 3.08-inch-diameter models. These pressures were generally determined from those within the balance shroud. For the latter part of the tests, however, the pressures were measured using small tubing mounted on each side of the exterior of the balance shroud and held in place by three pairs of wires.

Shadowgraph and oil-flow visualization tests were made with the present models. The shadowgraph pictures were obtained for each model simultaneously with the previously described force and moment measurements. The oil-flow technique described in reference 9 was utilized in the present tests. A satisfactory oil mixture was prepared using light vacuum-pump oil and titanium-dioxide pigment with oleic-acid as the dispersing agent in the approximate proportions, by volume, of 5:10:1, respectively. The tests were made only at a Mach number of 3.29 and, for the most part, with the sting support at 0° incidence. The models were sprayed with a thin layer of flat black lacquer to provide a contrasting background for the white titanium dioxide and a thin coating of the oil mixture was applied to the entire surface of the model. After the flow pattern was established at the given test conditions, the model was removed from the tunnel and photographed from several angles.

Reduction and Precision of Data

The force and moment data have been reduced to standard aerodynamic coefficients with the model cross-sectional area, based on the maximum diameter,

serving as the reference area. All the pitching-moment coefficients were determined with respect to the moment center shown in figure 1, using the maximum model diameter as the reference length. The force and moment coefficients correspond to the total measured forces and moments and thus include the effects of the pressures in the balance cavity. No attempt has been made to correct any of the measured data for the effects of these pressures, nor for any possible effects of the sting support itself.

In addition to any systematic errors that might be introduced by the sting support or the balance cavity pressures, the test data are also subject to random errors of measurement which affect the reliability of the data. The uncertainties in the measurement of the forces, moments, pressures, and test conditions have been reduced to standard deviations and are as follows:

$M = 5.45$ $R = 0.68\times10^6$		$M = 3.29$ $R = 1.07\times10^6$		$M = 3.29$ $R = 0.28\times10^6$	
C_N	±0.008	C_N	±0.003	C_N	±0.010
C_A	$\pm.004$	C_A	$\pm.002$	C_A	$\pm.005$
C_L	$\pm.008$	C_L	$\pm.003$	C_L	$\pm.010$
C_D	$\pm.004$	C_D	$\pm.002$	C_D	$\pm.005$
C_m	$\pm.005$	C_m	$\pm.002$	C_m	$\pm.006$
C_{p_b}	$\pm.0008$	C_{p_b}	$\pm.0003$	C_{p_b}	---
M	$\pm.02$	M	$\pm.02$	M	$\pm.02$
R	$\pm.02\times10^6$	R	$\pm.02\times10^6$	R	$\pm.02\times10^6$
α	$\pm.1^\circ$	α	$\pm.1^\circ$	α	$\pm.1^\circ$

RESULTS AND DISCUSSION

Force and Moment Data

The experimental results of the investigation are presented in standard coefficient form as functions of angle of attack. Graphs of C_N, C_A, C_m, C_L, C_D, L/D, and center-of-pressure location, x_{cp}/d, are presented in figures 4 and 5 for Mach numbers of 5.45 and 3.29, respectively. Corresponding values of these same aerodynamic functions given by modified Newtonian theory were computed by North American Aviation, Inc., and are also shown in figures 4 and 5. Values of the center-of-pressure location for a symmetrical model, determined in the usual manner by the quotient of $C_{m_{axis}}$ and C_N, are generally not trustworthy for angles of attack at or near 0° and 180° because of the reduced magnitude of C_N in these regions. These data are not shown in the figures. At 0° and 180° angle of attack, however, reliable theoretical and experimental values were obtained from the quotient of the local slopes $dC_{m_{axis}}/d\alpha$ and $dC_N/d\alpha$. A graph of balance-cavity pressure coefficient, C_{p_b}, is given in figure 6 for both supersonic Mach numbers.

The experimental data for a Mach number of 5.45 (fig. 4) agree well with the values given by modified Newtonian theory except in a few specific regions. The greatest discrepancies occur for C_m and C_A at angles of attack from about -25° to $+60^\circ$. The experimental values of C_D (or negative C_A) near 180° angle of attack are lower than the Newtonian values because the relieving effect of the rounded edge of the Apollo Command Module heat shield is not predicted by the theory. For a sharp edge, the experimental values would agree much better with those given by Newtonian theory (e.g., see ref. 10). The low theoretical values of C_A near 0° angle of attack, as compared with the experimental, are due to the inability of the Newtonian theory to predict accurately the pressures on a cone. If exact cone theory is used to predict the pressure coefficient on the conical portion of the body for zero angle of attack and modified Newtonian theory is used to define the pressure coefficient on the spherical portion of the blunt apex, a calculated C_A of 0.660 results, which is remarkably close to experiment. At a Mach number of 3.29 the over-all agreement between the experimental and Newtonian values, as evident in figure 5, is, on the whole, similar to that noted for the higher Mach number, but is somewhat poorer in scattered angle-of-attack ranges.

The effect of changing Reynolds number (fig. 5) is the most pronounced in the values of C_m and, correspondingly, x_{cp}/d. Some of the differences in C_m may be due to the differences in uncertainties in the values of C_m for the two test conditions. It should be observed that the pitching-moment data for the higher Reynolds number agrees much better with the Newtonian values, especially in the region of trim ($\alpha = 146^\circ$), than the data for the lower Reynolds number. The latter data indicate an angle of trim about 5° less than the Newtonian and higher Reynolds number values. It appears that the lower Reynolds number data are less reliable.

Force and moment data for a slightly different configuration of the Apollo Command Module are presented in reference 11 for Mach numbers from 1.5 through 10. This configuration differs from that of the present report only in the reduced radius of the blunted apex of the conical portion of the body, 0.059 instead of 0.10d as for the present configuration. The C_N and C_A data of the present report are in agreement with the corresponding data of reference 11 even though the latter correspond to somewhat higher Reynolds numbers and to the different apex radius. It is of interest to know also that very good agreement between the force and moment coefficients obtained by experiment and by modified Newtonian theory was found in reference 11 for a Mach number of 10 and a Reynolds number of 1.25 million.

Sting-Support Interference

Interference from a sting support can be influenced by sting length, diameter, and inclination, and can be affected by aerodynamic parameters, such as Mach number, Reynolds number, and location of boundary-layer transition. For the present tests an existing sting-support system was employed for which the length and the diameter were fixed. In the present report the inclination effects of this sting on the forces and moments of the Apollo Command Module

are of primary concern. It is also important to know whether or not the measured data may have been influenced to any appreciable extent by the length or diameter of this sting. To this end an attempt will be made to determine such information using fundamental data already available.

Effects of sting inclination.- The sting-inclination effects are evident from a comparison of the several data points shown in figures 4 and 5 for each angle of attack of the test. At first glance, these effects appear to be of the order of magnitude of the standard deviations of the aerodynamic coefficients presented earlier in the Reduction and Precision of Data section of this report. Repeated tests of the models (data not presented), however, have shown that the indicated effects are valid and are generally somewhat larger in magnitude than the noted standard deviations, whereas the repeatability of the data is, for the most part, well within these deviations.

Noticeable effects of sting-support inclination up to $\pm 30^{\circ}$ are apparent in the data of figures 4 and 5 for Mach numbers of 5.45 and 3.29, respectively. Only for the pitching-moment coefficients, however, are these effects substantial over most of the angle-of-attack range. The effects of sting inclination are apparent for the other data of these figures only in small ranges of angles of attack and are generally much smaller than for the pitching-moment coefficients. Sting inclination appears to have affected C_A and C_L the least over the entire angle-of-attack range. Even if the sting inclination were limited to a $\pm 10^{\circ}$ range, the pitching-moment coefficients as well as the other aerodynamic data for a Mach number of 5.45 indicate that no appreciable reduction in the magnitude of the effects would result. Less effects of sting inclination are evident in the data for the 60° and 80° offset models in figure 5 for a Mach number of 3.29 than are indicated in the corresponding data in figure 4 for a Mach number of 5.45.

A comparison of the data for the two Reynolds numbers shown for angles of attack of 150°, 155°, and 160° reveals that the effects of sting inclination are reduced for the higher Reynolds number. This reduction is also more apparent for the pitching-moment coefficients.

It has been noted for a Mach number of 5.45 and a Reynolds number of 0.68 million that the aerodynamic data, and especially the pitching-moment coefficients, are influenced by sting-support inclinations as small as $\pm 10^{\circ}$. These effects, however, may be of little practical concern for the Apollo Command Module except for angles of attack in the vicinity of trim. In order to obtain data that are free from the effects of sting inclination for such angles of attack, the sting support, most likely, should be positioned so as to aline closely with the location and direction the free wake would have immediately behind the model. The inclination of the free wake adjacent to the Apollo Command Module is, of course, not zero relative to the free-stream direction throughout the angle-of-attack range. Measurements of the wake inclination near the base of approximate models of the Apollo Command Module and the Mercury capsule have been made from shadowgraph pictures obtained during free-flight tests at Mach numbers from about 11 to 18 and from 3 to 4. These pictures were obtained in two research facilities of the Hypersonic Free-Flight Branch of the Ames Research Center. As a matter of interest the

shadowgraph pictures are presented in figures 7 and 8, and approximate wake-inclination measurements together with appropriate test data are given in the following table:

Approximate model	M	R	α, deg	Approximate wake inclination near body, relative to free-stream direction (positive when inclined downward), deg	Shadowgraph figure no.
Apollo	18.0	0.52×10^6	22.6	1	7(a)
	16.6	$.72\times10^6$	42.8	-3	7(b)
	17.8	$.51\times10^6$	-80.4	-2	7(c)
	16.6	$.48\times10^6$	86.3	3	7(d)
	11.4	$.65\times10^6$	140.0	-1	7(e)
	13.6	$.77\times10^6$	-148.8	2	7(f)
Mercury	4.0	$.58\times10^6$	33.1	0	8(a)
Mercury	3.6	$.52\times10^6$	54.9	-2	8(b)
Apollo	3.3	$.58\times10^6$	144.5	5	8(c)
Apollo	3.7	$.58\times10^6$	-152.5	-4	8(d)

The wake inclination is much more difficult to ascertain from the shadowgraph pictures for the higher Mach numbers than for the lower because of the differences in visibility of the wake. Accordingly, the accuracy of the measured inclinations given above is estimated to be about $\pm2^\circ$ for the higher Mach numbers and about $\pm1^\circ$ for the lower. From the values given it appears that the magnitude of the wake inclination is generally small and is not greater than about $\pm5^\circ$.

The present experimental data for the Apollo Command Module indicate trim or near trim at angles of attack from about 60° to 90° and at about 150°. If the wake-inclination data given for a Mach number of about 4 are appropriate for a Mach number of 5.45, it can be inferred that the data for the 60° offset model with the sting inclined -5° or 0° ($\alpha = 55^\circ$ or 60°) and the data for the 140° offset model with the sting inclined at 5° ($\alpha = 145^\circ$) are essentially free from sting-inclination effects. As a consequence the angles of trim indicated by the pitching-moment data for a Mach number of 5.45 may be accepted with more confidence.

It is suggested in reference 4 that changes in the magnitude of experimental slender-body base pressures would reflect corresponding changes in support interference, because each depends strongly on Reynolds number and the location of transition. If such should be the case for flow over a blunt body, the variations in base-pressure measurements would indicate corresponding variations in sting interference. It is observed in figure 6 that the variations of balance-cavity pressure coefficient with angle of attack are generally small and irregular for each model, and that the variations for a

Mach number of 3.29 are slightly larger than the corresponding variations for a Mach number of 5.45. It is apparent, therefore, that the relationship between the magnitudes of the pressure coefficients for each of the models and for each Mach number does not correlate with the effects of sting inclination as observed in the data of figures 4 and 5.

Effects of sting length.- It is believed that a basis for determining a practical length sting behind a short, blunt body, such that no appreciable interference will be introduced to the flow over the body as a result of the structure supporting the sting, can be established from a knowledge of the actual wake characteristics for the body. It is well known that supersonic flow expands over the base or afterportion of a body, and subsequently recompresses downstream forming trailing shock waves and a region in the wake comparable to the throat of a nozzle. The throat region is just upstream of the origin of the trailing waves. (See sketch.) In the mixing theory of Crocco and Lees reported in reference 12, disturbances downstream of a "critical point" near the throat do not propagate upstream ahead of this point. This feature of the flow has been confirmed experimentally for slender bodies, as reported in reference 4. No interference due to the sting length was evident when the sting terminated somewhat downstream of the throat region in the wake. It was reasoned that this property of the flow should remain unchanged for a sting-supported blunt body. Accordingly, the sting of the present investigation can be judged free of interference due to its length if the sting terminates well downstream of the location of the origin of the trailing shock waves. Reference is made to the origin of the shock waves rather than the location of the wake throat because the two occur at essentially the same position, and the shock waves are much more apparent in shadowgraph pictures, especially for high Mach numbers.

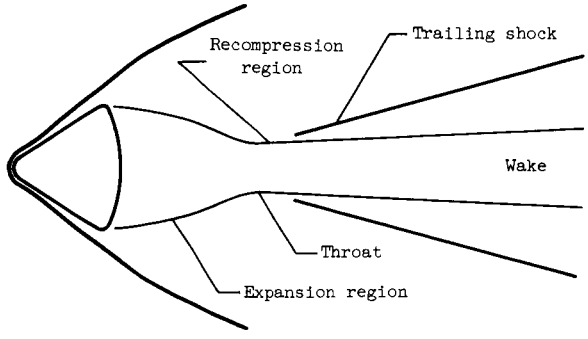

Representative shadowgraph pictures for the Apollo Command Module are presented in figures 9 and 10 for Mach numbers of 5.45 and 3.29, respectively.[1] Only those pictures for sting inclinations between approximately $\pm 10^{\circ}$ were considered. Unfortunately, the field of view in the pictures extends downstream of the body only about one-half the length of the undisturbed portion of the sting.

It is inferred from a study of the shadowgraph pictures that the sting used during the tests was sufficiently long that interference effects on the measured data would be negligible for sting inclinations to at least $\pm 10^{\circ}$. Even with the restricted field of view, the origin of both trailing shock waves is visible in the pictures for $\alpha = 60^{\circ}$ at a Mach number of 5.45, and

[1]During the tests associated with the lower two photographs of figure 9(d) and in all four of figure 10(a), the exterior tubing was employed for measuring the balance-cavity pressures. Accordingly, the three pairs of wires that held the tubing on the sides of the balance shroud are evident in these photographs.

especially for all the angles shown for a Mach number of 3.29, except for 175° at the lowest Reynolds number. The origin of at least one of the trailing waves is observed in most of the remaining pictures, suggesting that the other wave must be close behind but out of the field of view. Accordingly, it was reasoned that the origin of the trailing shock waves was well upstream of the termination of the sting support and, therefore, the flow over the models was free of interference due to the sting length.

From the theory of Crocco and Lees (ref. 12) it is apparent that the length of sting required for noninterference is directly proportional to the distance of the wake-throat region from the body. Kavanau in reference 13 indicates that the position of the wake-throat region is determined by the location of transition relative to this region. The throat is farthest from the body when transition occurs within the throat. When transition moves either upstream or downstream from this location, accompanying an increase or a decrease in Reynolds number, respectively, the wake-throat region always moves nearer the body. Available sting-length interference data substantiate such a movement of the wake-throat region with variation in Reynolds number (e.g., see refs. 4 and 13). Inasmuch as it has been shown earlier in the present report that the higher Reynolds number data were influenced less by sting inclination than were the data for the lower Reynolds number, it is recommended that an increase in Reynolds number be employed to move the wake throat nearer the body which, in turn, will shorten the length of sting necessary for noninterference.

Effects of sting diameter.- The effects of sting diameter cannot be evaluated directly from the present data since only one ratio of sting diameter (shroud diameter) to model diameter (0.28) was employed in the investigation, and no other basis is known by which such effects might be evaluated. The only known published data pertaining to sting-diameter effects associated with a blunt body are those of reference 7 for a Mach number of 19.4. These data show appreciable diameter effects even for small sting supports. This result is in accord with the existing sting-diameter information for slender bodies with turbulent boundary layers. Slender-body data for laminar boundary layers, however, have shown generally little effect of the diameter.

The influence of sting diameter in any support system appears mainly as a change in the base pressure on the model. For short blunt bodies this change may be felt over the entire lee portion of the model. Even though the influence of sting diameter might be small, the integrated effects on such a large part of the model could be substantial. It is believed, however, that the sting-diameter effects on the test data of the present report are of the order of magnitude of the accuracy of the experimental data.

Surface-Flow Characteristics

A brief study of some of the flow characteristics on the surface of the Apollo Command Module was undertaken for a Mach number of 3.29 to detect, if possible, any interference of the sting support on the local flow, and also to determine the effects of angle of attack on the location of the stagnation

point and of separation. Oil-flow photographs showing several views of the models at angles of attack from 0° to 180° are presented in figure 11. Good detail of the flow directions over the surface, and the locations of the stagnation and separated regions are apparent. Of interest is the evidence of body vortices shown in view 4 for angles of attack of 40° and 60° (figs. 11(b) and 11(c)). Vortices apparently formed at some angle of attack greater than 33° (the angle of attack for which the edge of the conical portion of the body is alined with the free-stream direction) and existed through 60° but were not evident on the model surface for an angle of attack of 80°. The vortices may still exist in the flow at this latter angle of attack, but may be too far from the surface to form a pattern in the oil. The only evidence of possible interference on the surface flow due to the presence of the sting support is seen in view 3 for an angle of attack of 60°. This appears as a pair of small disturbed areas adjacent to the sting support. These disturbances, however, are believed to be associated with the body vortices rather than with the sting.

The location of the stagnation point for each angle of attack has been determined from the photographs and is presented in figure 12. In this figure the location is shown on the profile of the Apollo Command Module and in graphical form as the radial distance from the body axis of symmetry. The symbols shown in the graph indicate various measurements taken from the models or from photographs. Predicted locations of the stagnation point were obtained from reference 14 for the Apollo Command Module at angles of attack from 130° to 180°, and are also presented in the graph of figure 12. The experimental trend with angle of attack is predicted fairly well, but the experimental values are about 4 to 7 percent lower than calculated.

The regions of separation on the conical and large spherical (heat-shield face) portions of the Apollo Command Module have been determined from the photographs of figure 11 and are shown in figure 13. The boundaries of flow separation for several angles of attack are shown in the upper and lower parts of the figure, respectively, on a developed surface of the conical portion of the body and on a view of the heat-shield face along the axis of symmetry toward the apex of the conical portion of the body.

On the conical portion of the body at an angle of attack somewhat above 33° the flow separates within an essentially Λ-shaped boundary that widens as the angle of attack is increased. For angles of attack above about 100° the lower portions of the boundaries of separation spread abruptly in a lateral direction toward the rim of the heat-shield face. For angles of attack between 147° and 180°, the flow separates over the entire conical part of the body, of course.

On the heat-shield face the flow is separated over essentially the entire surface for angles of attack below about 40° and over part of the surface for angles of 60° and 80°. There are no significant regions of separation on this surface for angles of attack greater than about 100°.

CONCLUDING REMARKS

The present study has shown that the effects of sting-support inclination on the force and moment characteristics of the Apollo Command Module were apparent for a Mach number of 5.45 and a Reynolds number of 0.68 million, even for sting inclinations no greater than $\pm 10^{\circ}$. These effects were substantial, however, only for the pitching-moment coefficients. The effects of increasing Reynolds number from 0.28 million to 1.07 million for a Mach number of 3.29 suggest that the interference due to sting inclination might be eliminated at higher Reynolds numbers. Even for the above Reynolds numbers, it is believed that data free of sting-inclination effects can be obtained, provided the model is mounted at the desired angle of attack on a sting support which is inclined to correspond with the direction a free wake would have immediately behind the model. Accordingly, for angles of attack in the vicinty of trim at a Mach number of 5.45, it was inferred that the data for the 60° offset model with the sting inclined at -5° or 0° ($\alpha = 55^{\circ}$ or 60°) and the data for the 140° offset model with the sting inclined at 5° ($\alpha = 145^{\circ}$) are essentially free from sting-inclination effects.

The sting employed during the present tests was judged to be sufficiently long, for sting inclinations to at least $\pm 10^{\circ}$, to prevent appreciable interference on the experimental force and moment data as a result of the structure which supported the sting. This judgement was based on the locations of the trailing shock waves evident in the shadowgraph pictures. Sufficient criteria were not available for determining the effects of the sting diameter, although such effects are believed to be small.

The experimental force and moment characteristics of the Apollo Command Module for Mach numbers of 5.45 and 3.29 generally agreed well with the corresponding values given by modified Newtonian theory, except in a few specific ranges of angle of attack. The greatest discrepancies occurred for the pitching-moment and axial-force coefficients at angles of attack from about -25° to $+60^{\circ}$.

The surface-flow photographs of the models of the Apollo Command Module for a Mach number of 3.29 not only permit a detailed study of the directions of flow over the entire surface, but also provide information on the location of the stagnation point and the regions of separation as a function of angle of attack. The variation with angle of attack of the stagnation point over the large spherical portion (heat-shield face) of the body was predicted moderately well by an empirical method.

Ames Research Center
National Aeronautics and Space Administration
Moffett Field, Calif., Dec. 4, 1964

REFERENCES

1. Chapman, Dean R.: An Analysis of Base Pressure At Supersonic Velocities and Comparison With Experiment. Appendix B. NACA Rep. 1051, 1951.

2. Love, Eugene S.: A Summary of Information on Support Interference at Transonic and Supersonic Speeds. NACA RM L53K12, 1954.

3. Lee, George; and Summers, James L.: Effects of Sting-Support Interference on the Drag of an Ogive-Cylinder Body With and Without a Boattail at 0.6 to 1.4 Mach Number. NACA RM A57I09, 1957.

4. Whitfield, Jack D.: Critical Discussion of Experiments on Support Interference at Supersonic Speeds. AEDC-TN-58-30, 1958.

5. Rebuffet, P.: Effets De Supports Sur L'Ecoulement A L'Arriere D'Un Corps. AGARD Rep. 302, 1959.

6. Peckham, D. H.: Exploratory Tests on Sting Interference at a Mach Number of 6.8. British R.A.E. TN Aero. 2721, 1960.

7. Watson, Ralph; and Wagner, Richard D., Jr.: Pressure Distribution at a Mach Number of 24.5 on a Symmetrical Blunt-Faced Reentry Body at Angles of Attack From 0° to 40° in Helium, Including an Investigation of Afterbody Sting Effects. NASA TM X-841, 1963.

8. Hayes, Wallace D.; and Probstein, Ronald F.: Hypersonic Flow Theory. Academic Press, N. Y., 1959, pp. 3-8.

9. Stanbrook, A.: The Surface Oil Flow Technique as Used in High Speed Wind Tunnels in the United Kingdom. British R.A.E. TN Aero. 2712, 1960.

10. Sammonds, Robert I.; and Dickey, Robert R.: Effectiveness of Several Control Arrangements on a Mercury-Type Capsule. NASA TM X-579, 1961.

11. Gray, J. Don; and Jones, J. H.: Force and Pressure Tests on Apollo Configurations at Mach 1.5 Through 10. AEDC-TDR-63-17, 1963.

12. Crocco, Luigi; and Lees, Lester: A Mixing Theory for the Interaction Between Dissipative Flows and Nearly Isentropic Streams. J. Aero. Sci., vol. 19, no. 10, Oct. 1952, pp. 649-676.

13. Kavanau, L. L.: Base Pressure Studies in Rarefied Supersonic Flows. Univ. of Calif. Inst. Engr. Res. Rep. HE-150-125, 1954.

14. Kaattari, George E.: Shock Envelopes of Blunt Bodies at Large Angles of Attack. NASA TN D-1980, 1963.

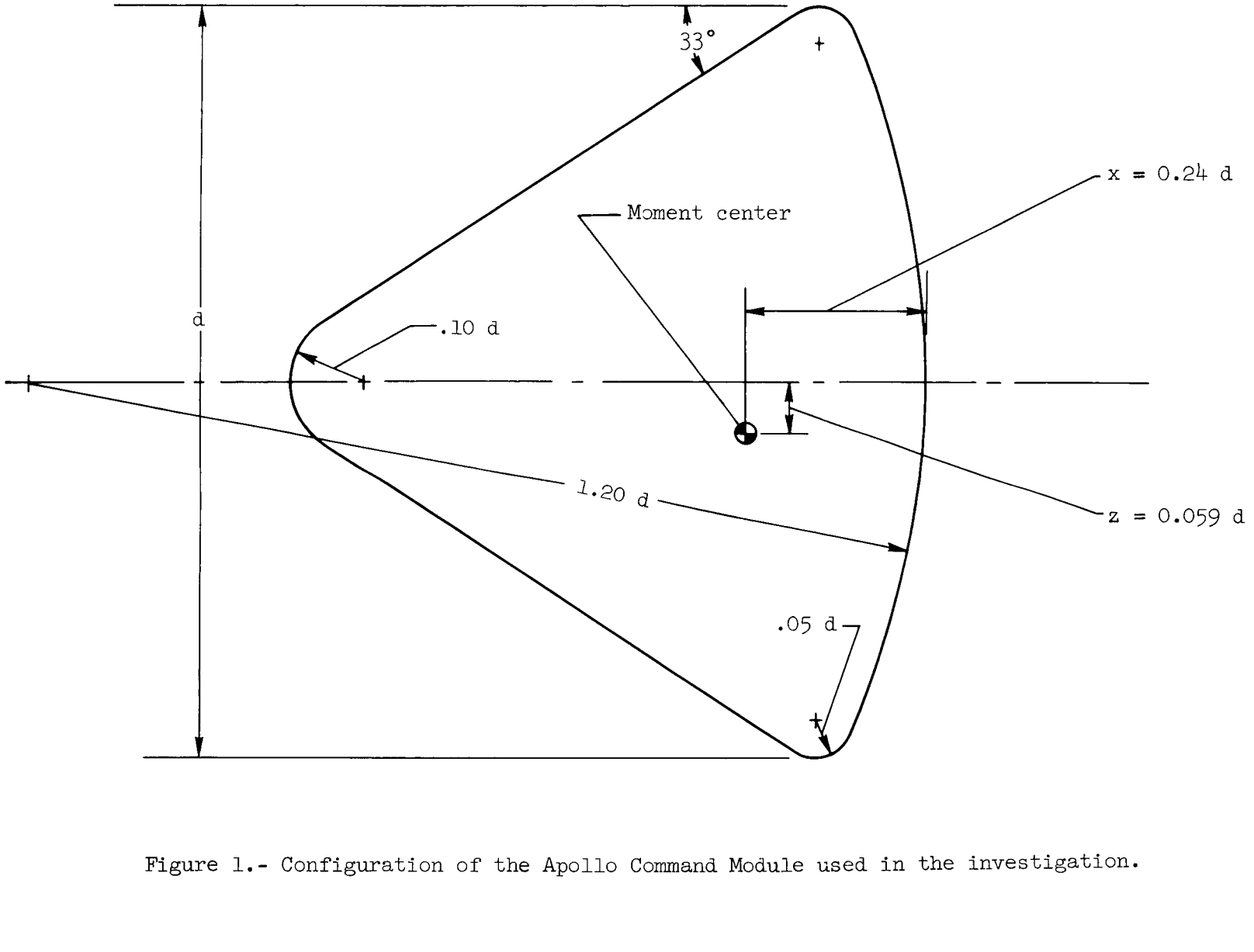

Figure 1.- Configuration of the Apollo Command Module used in the investigation.

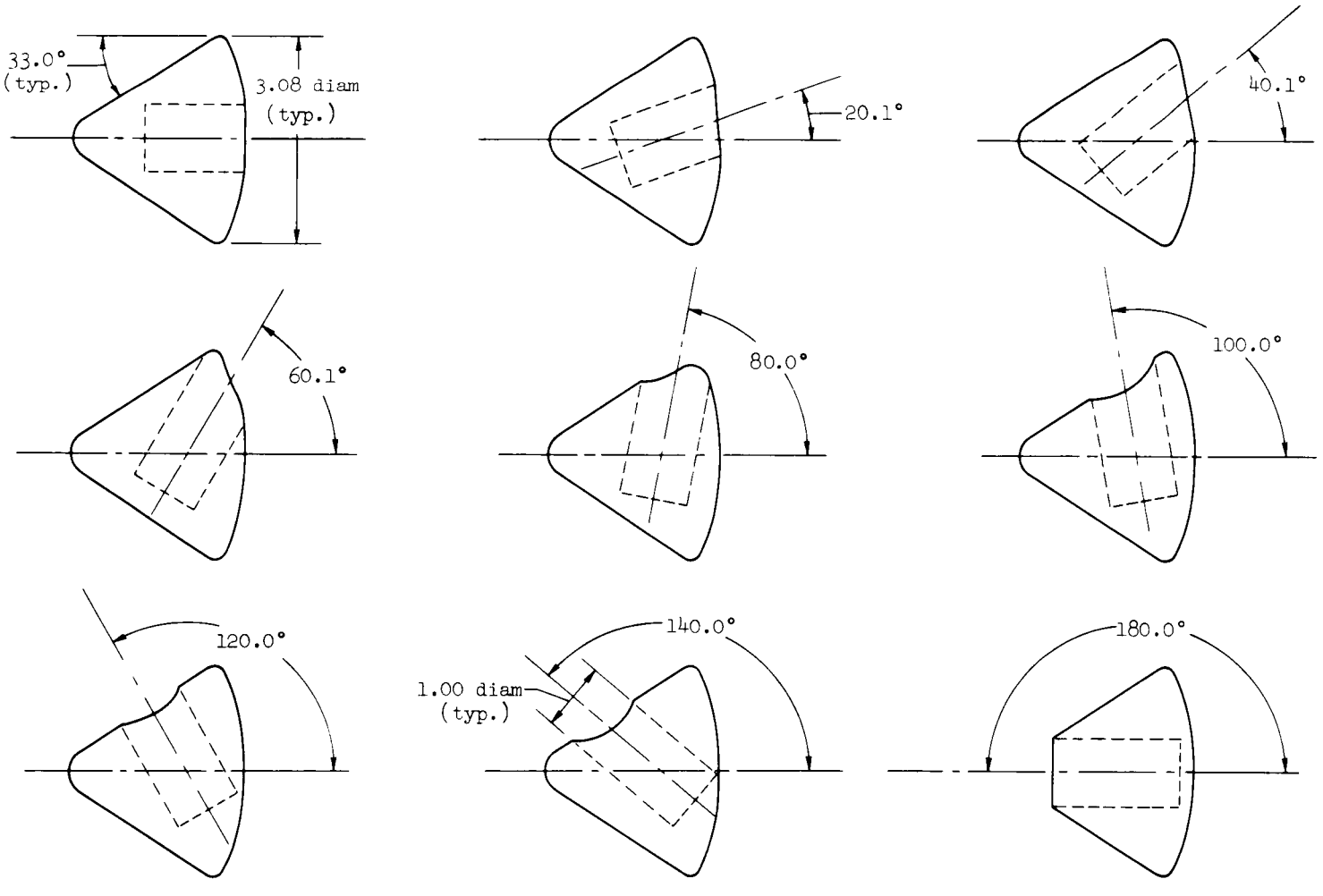

All dimensions in inches except as noted

(a) The 3.08-inch-diameter models.

Figure 2.- Illustration of the models tested.

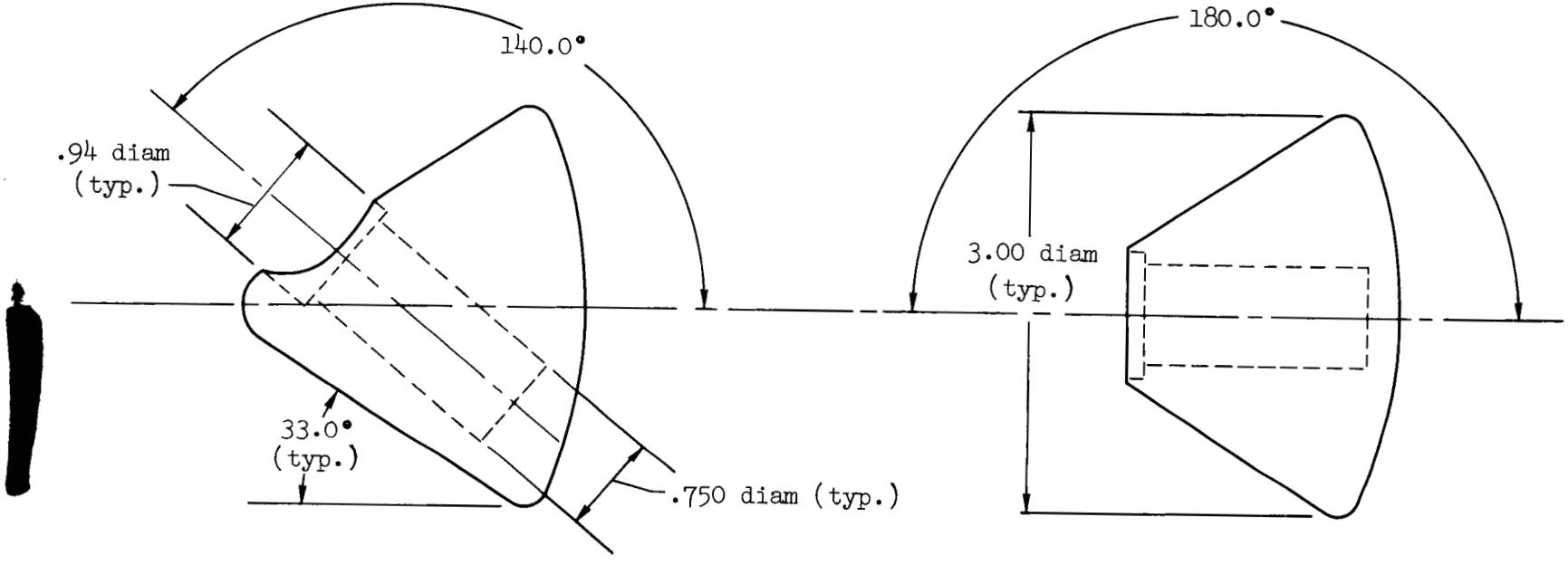

All dimensions in inches except as noted

(b) The 3.00-inch-diameter models .

Figure 2.- Concluded.

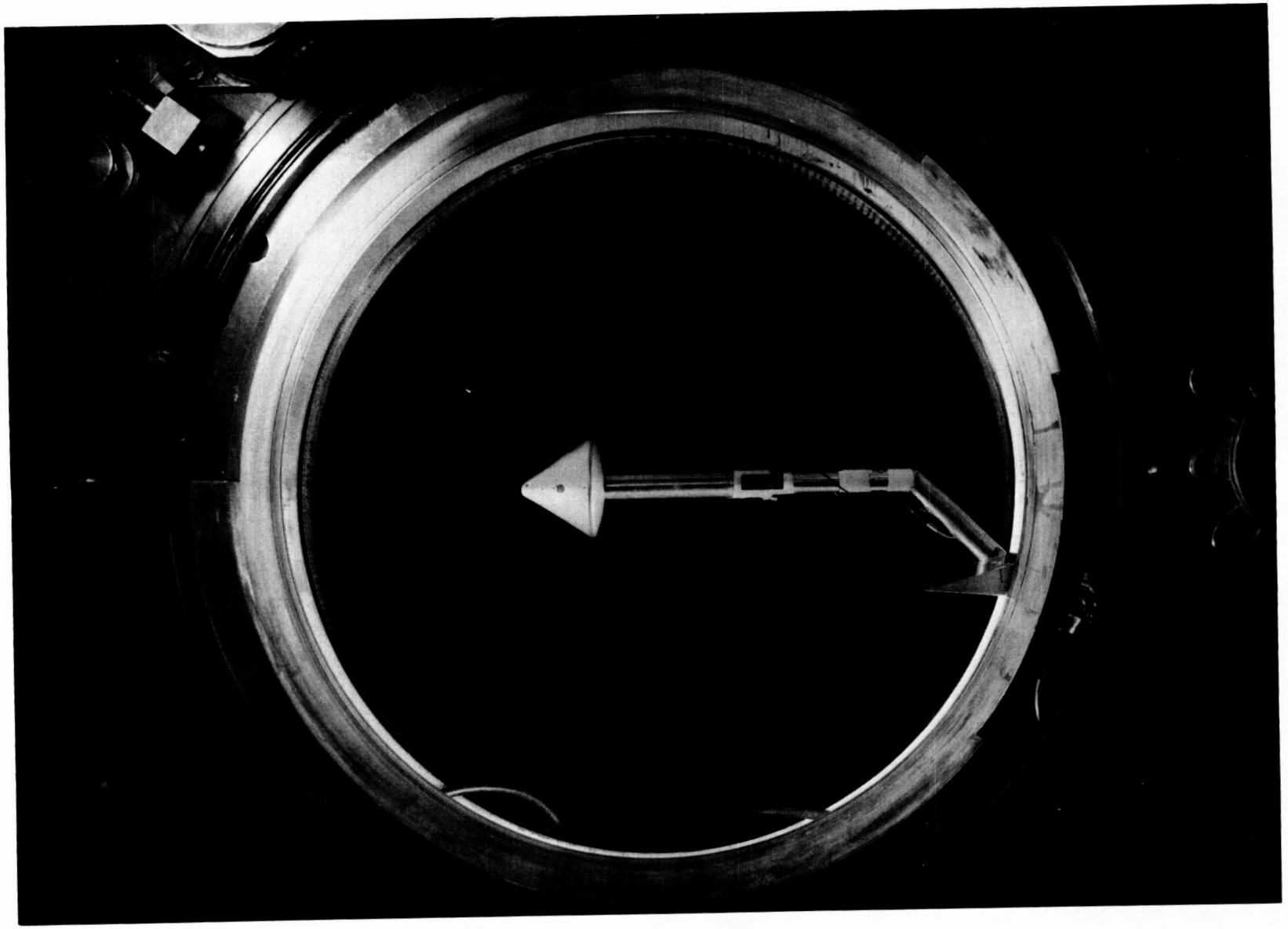

A-30835

Figure 3.- The 0° offset model mounted in the Ames 1- by 3-Foot Supersonic Wind Tunnel.

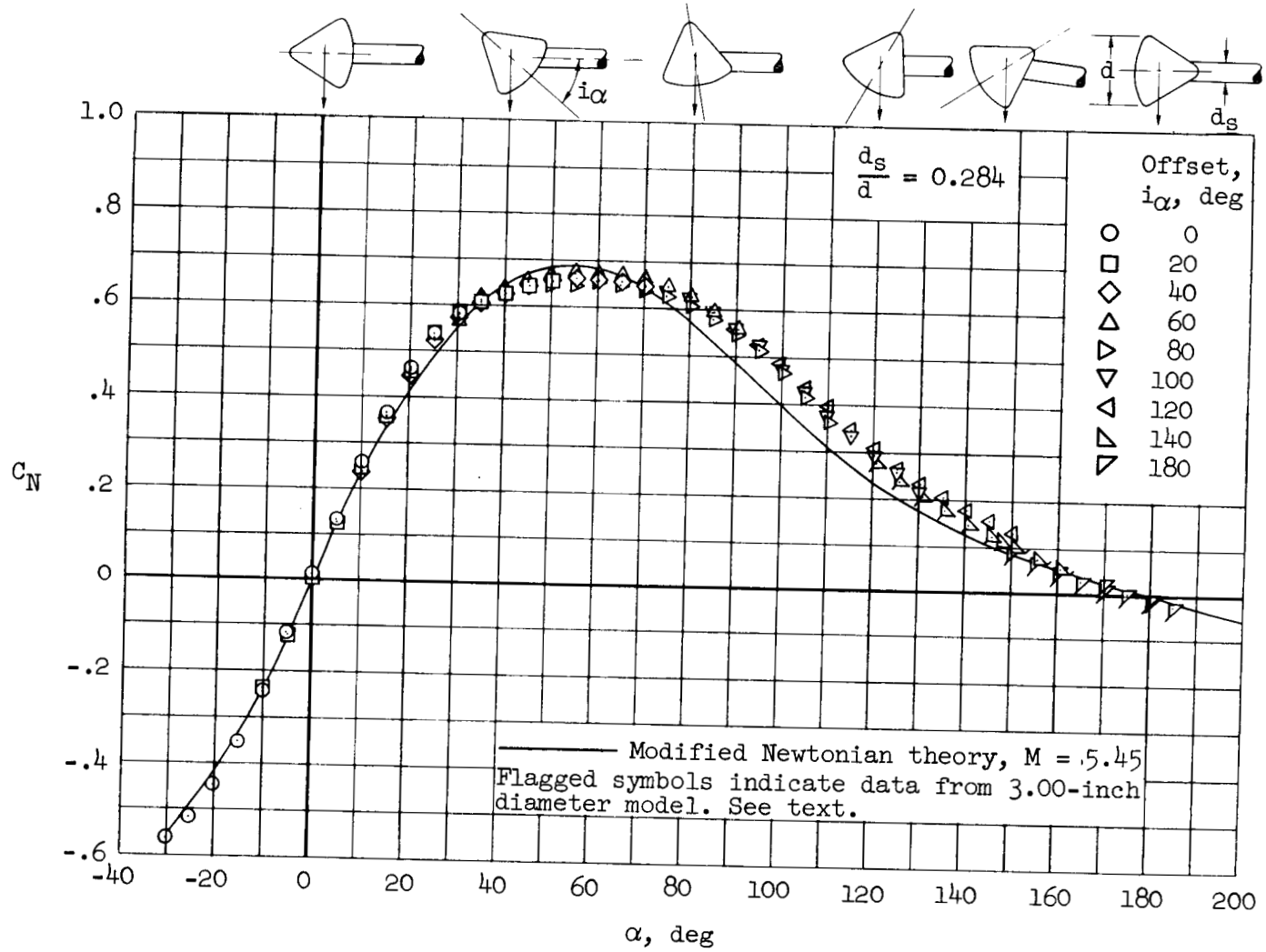

(a) C_N versus α

Figure 4.- Aerodynamic characteristics of an early configuration of the Apollo Command Module for a Mach number of 5.45 and a Reynolds number of 0.68 million.

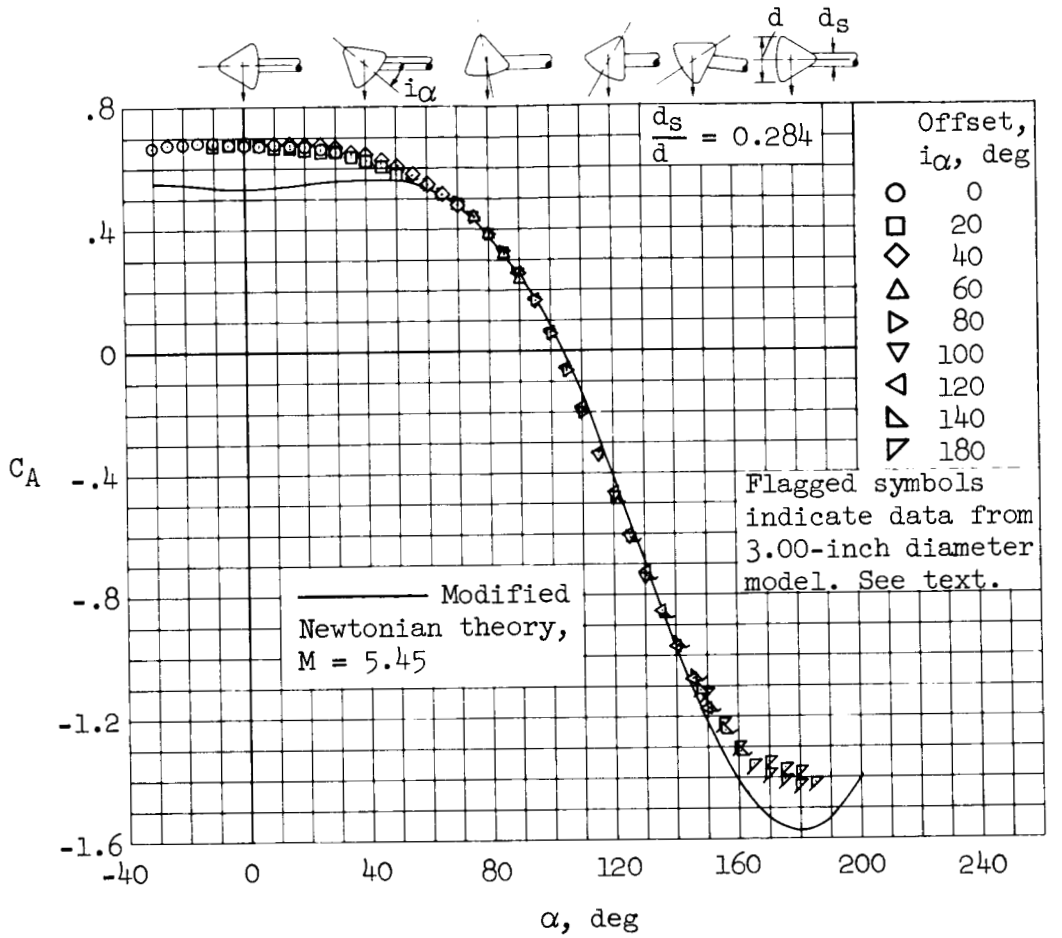

(b) C_A versus α

Figure 4.- Continued.

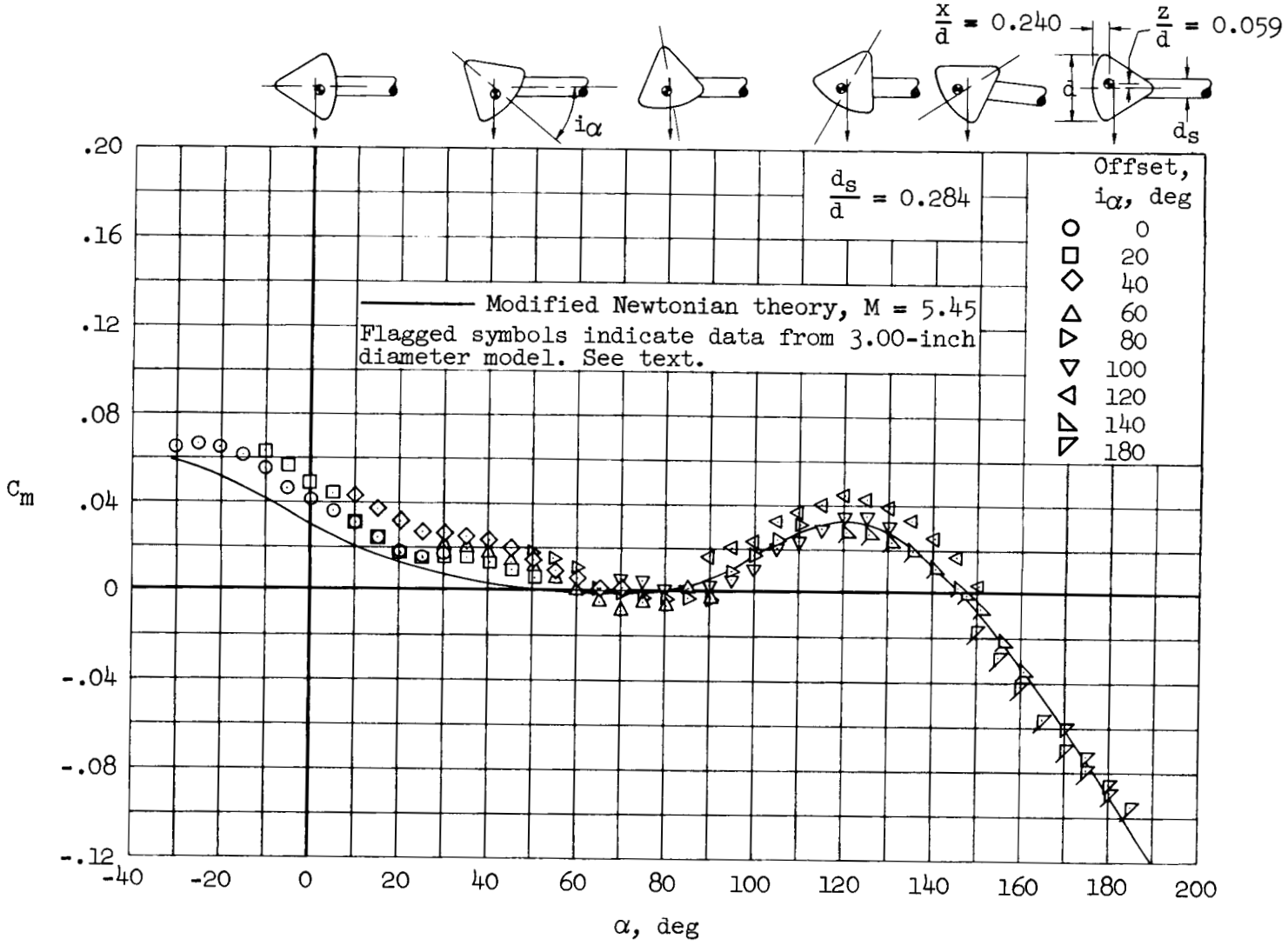

(c) C_m versus α

Figure 4.- Continued.

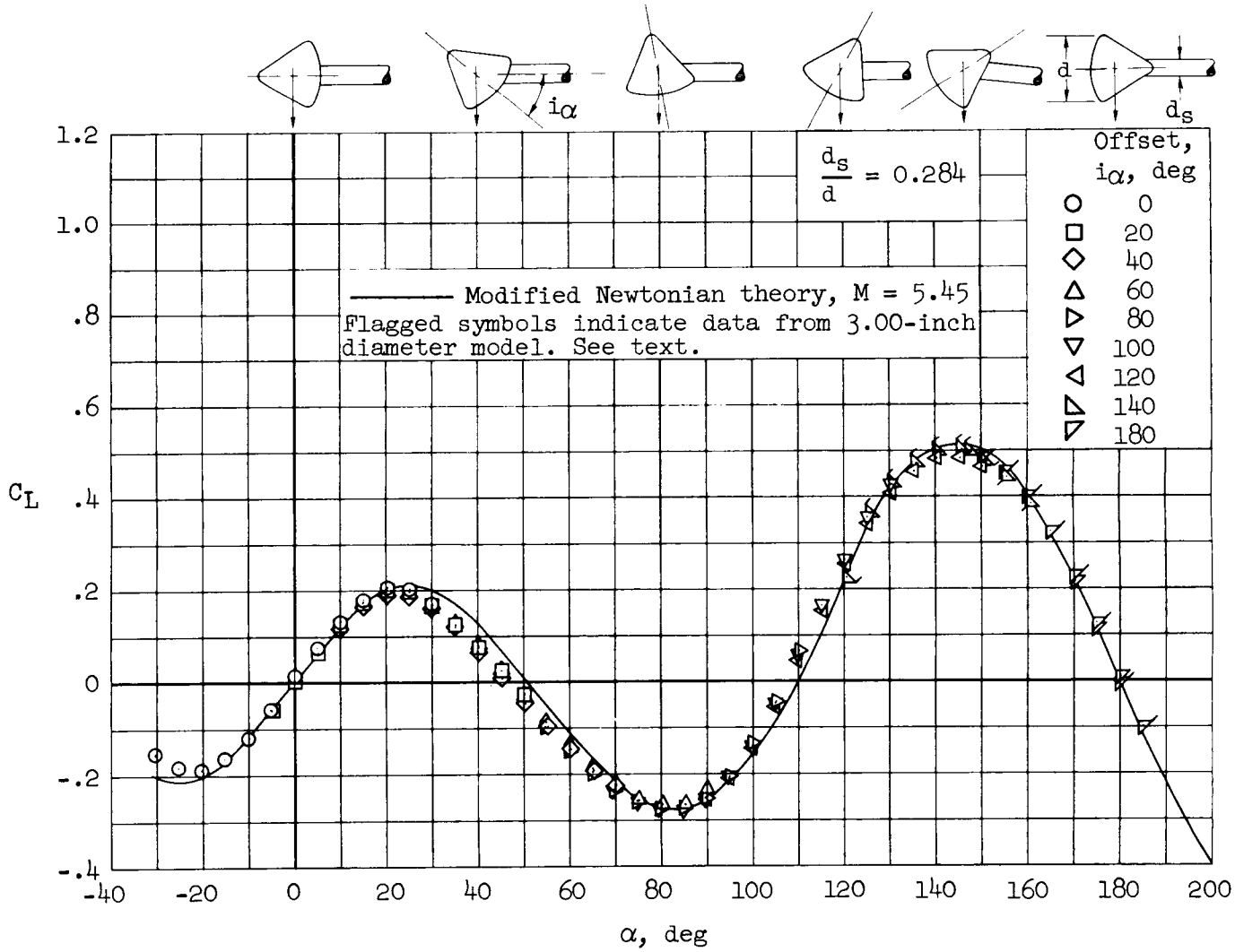

(d) C_L versus α

Figure 4.- Continued.

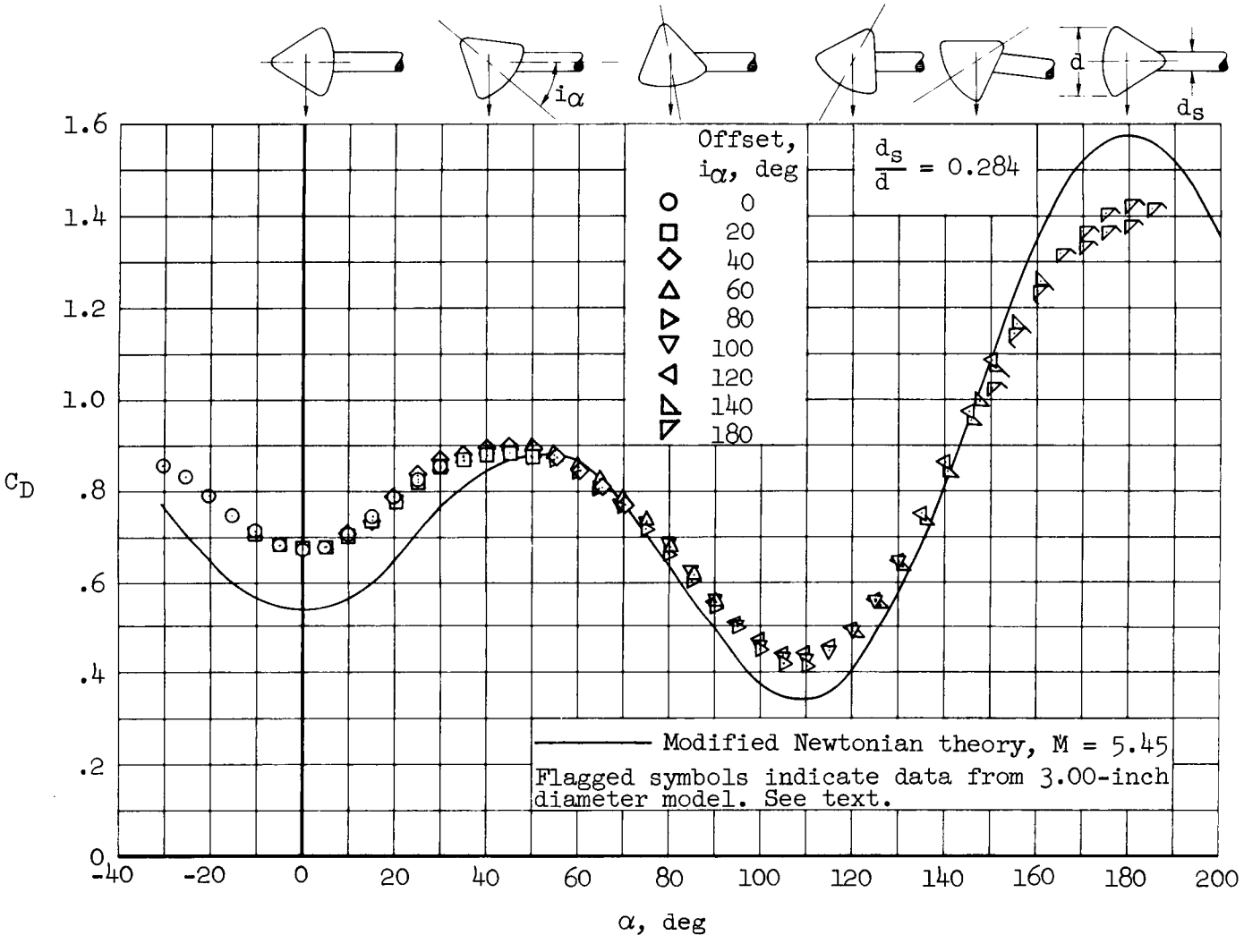

(e) C_D versus α

Figure 4.- Continued.

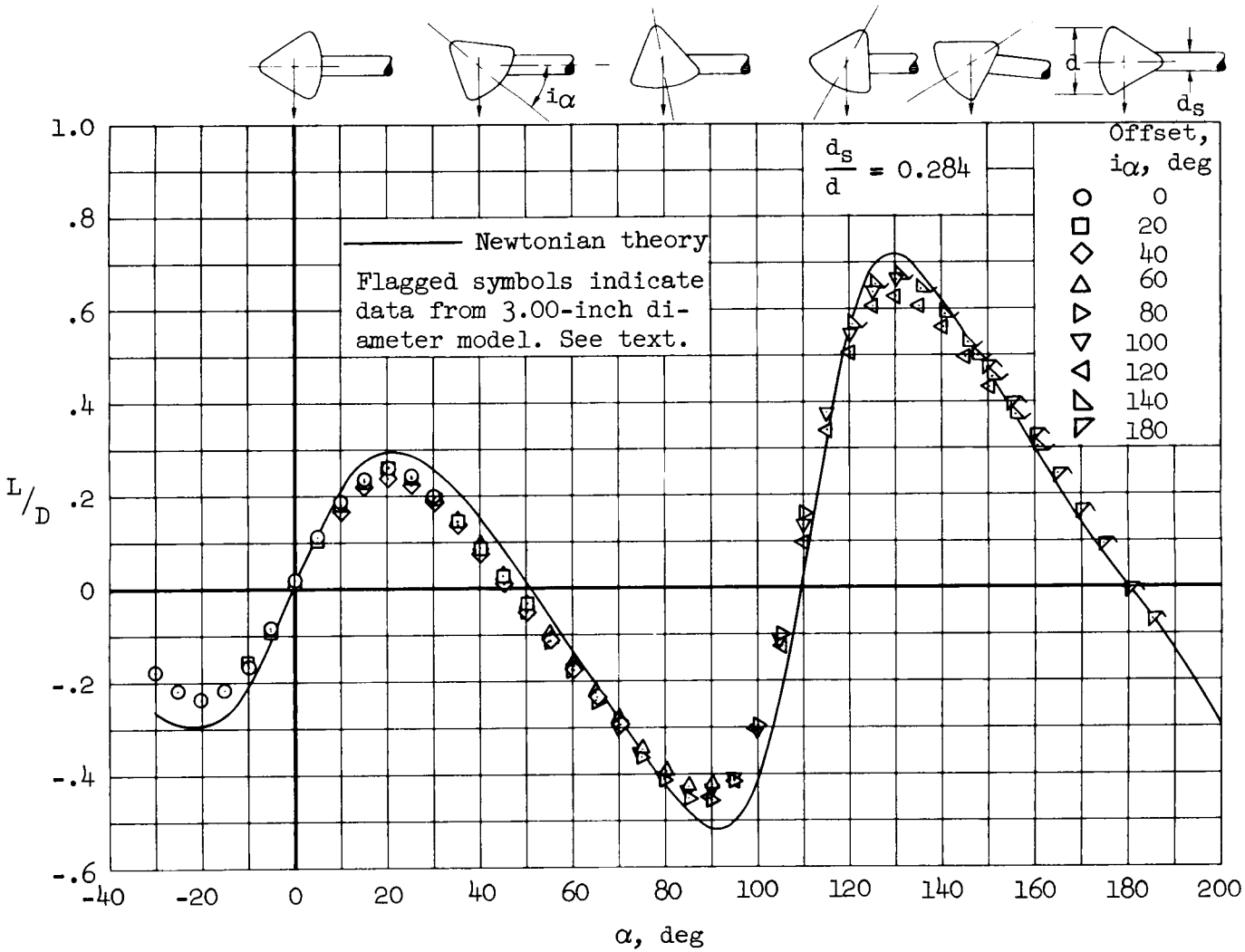

(f) L/D versus α

Figure 4.- Continued.

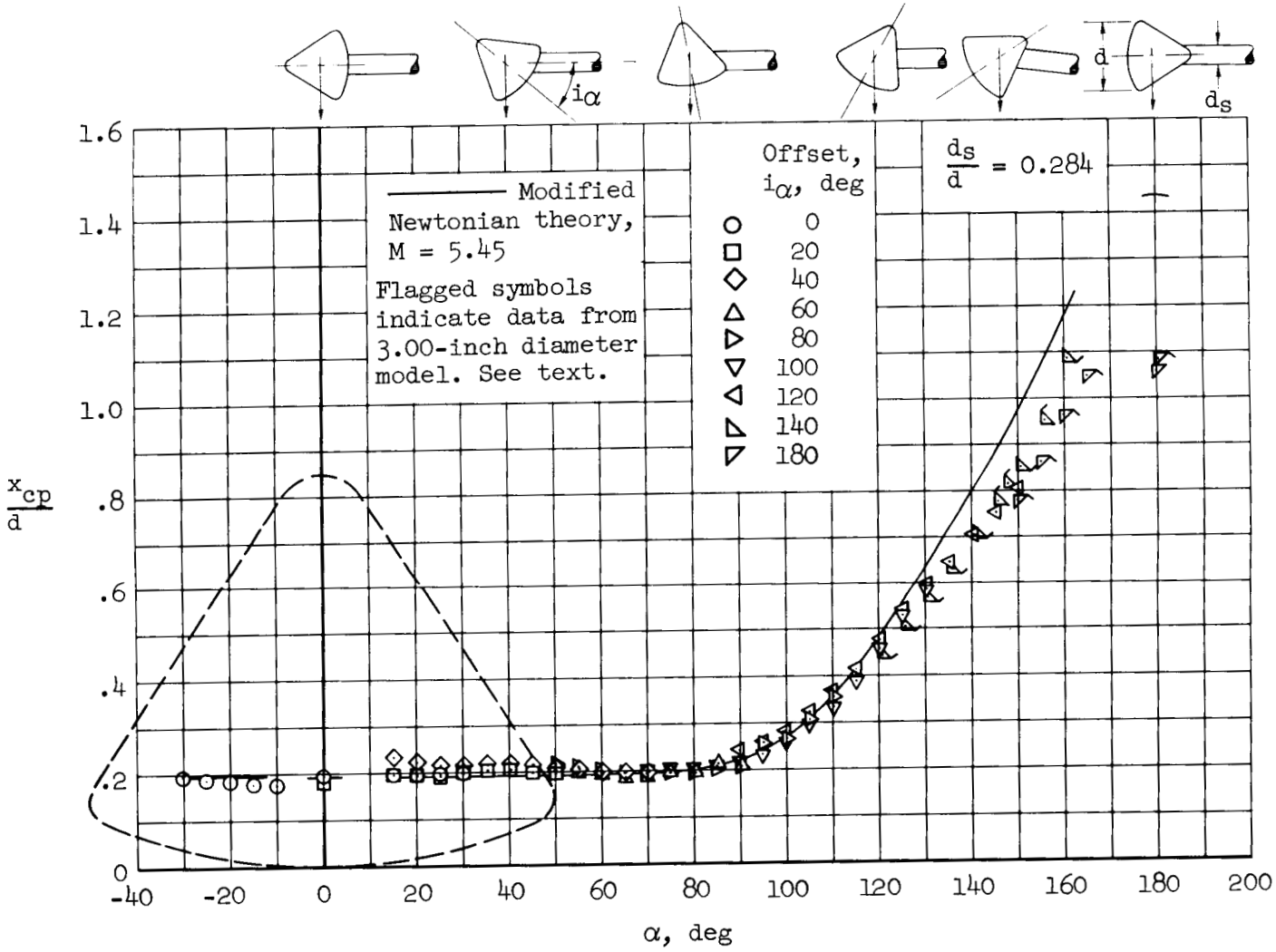

(g) $\frac{x_{cp}}{d}$ versus α

Figure 4.- Concluded.

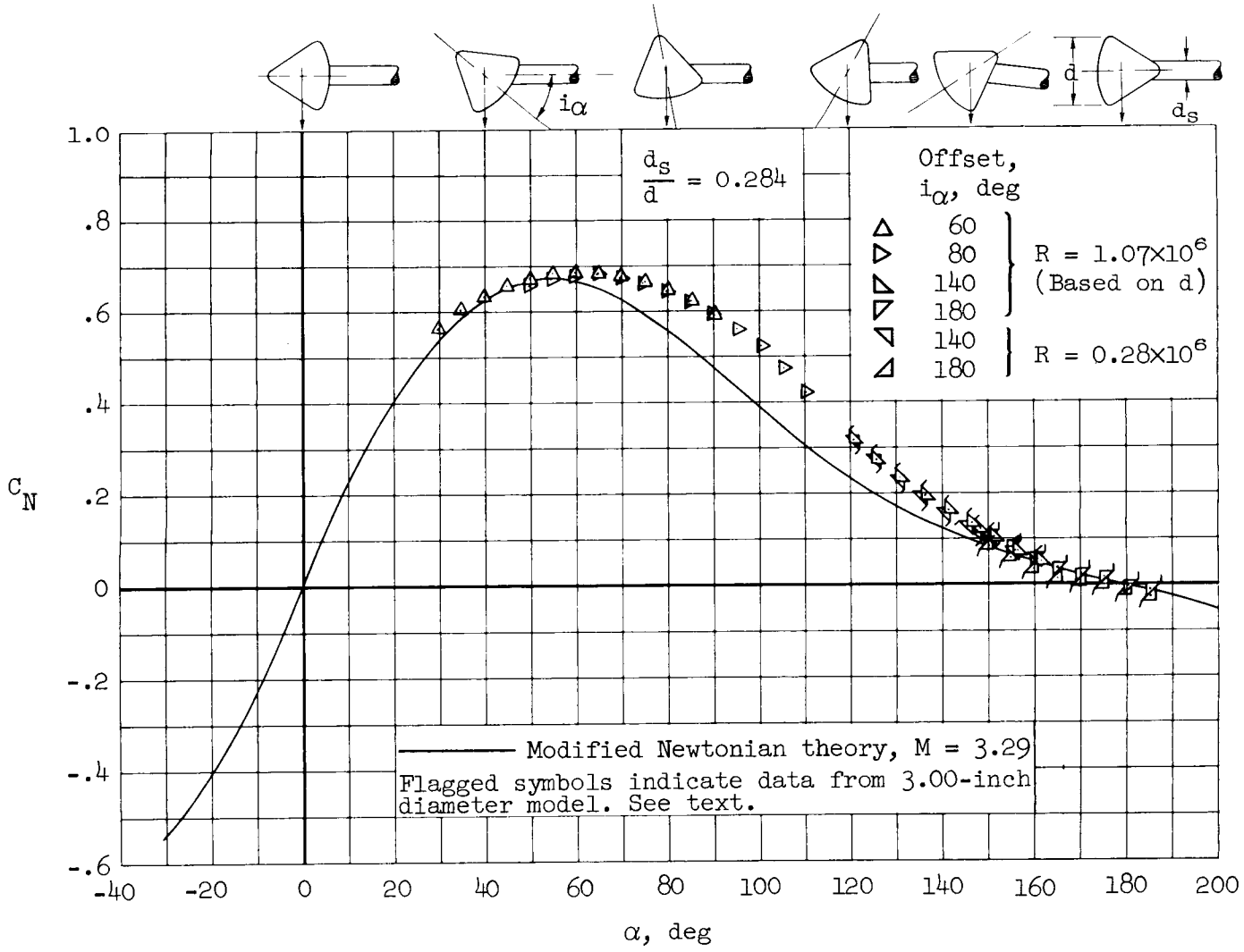

(a) C_N versus α

Figure 5.- Aerodynamic characteristics of an early configuration of the Apollo Command Module for a Mach number of 3.29 and for Reynolds numbers of 1.07 million and 0.28 million.

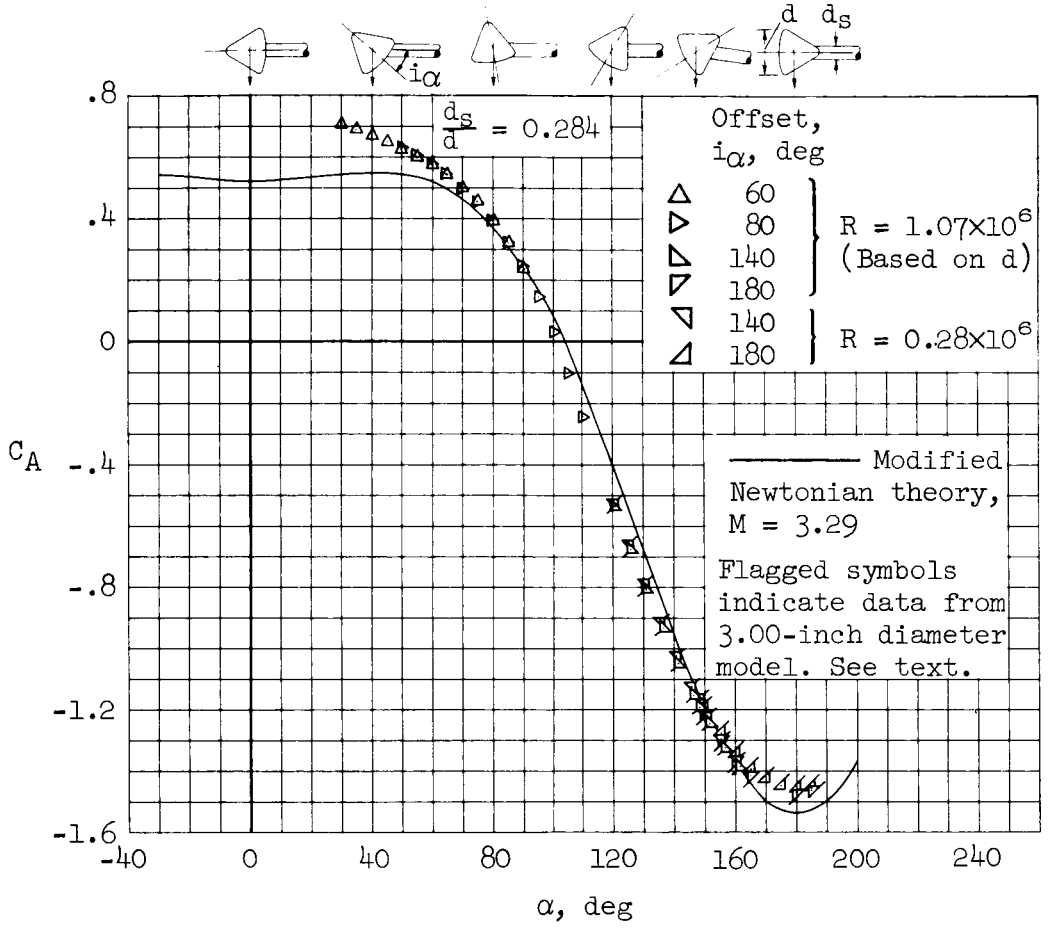

(b) C_A versus α

Figure 5.- Continued.

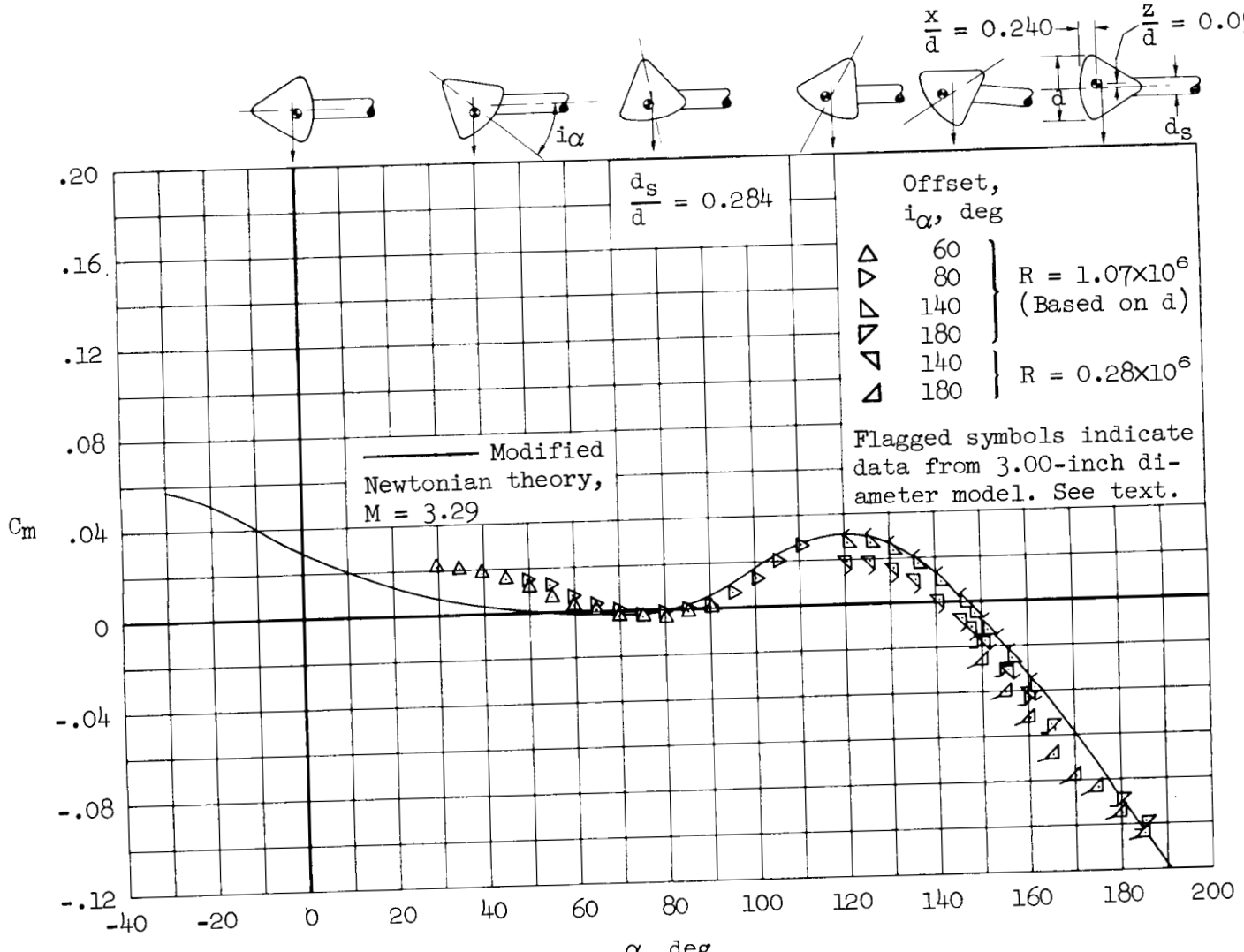

(c) C_m versus α

Figure 5.- Continued.

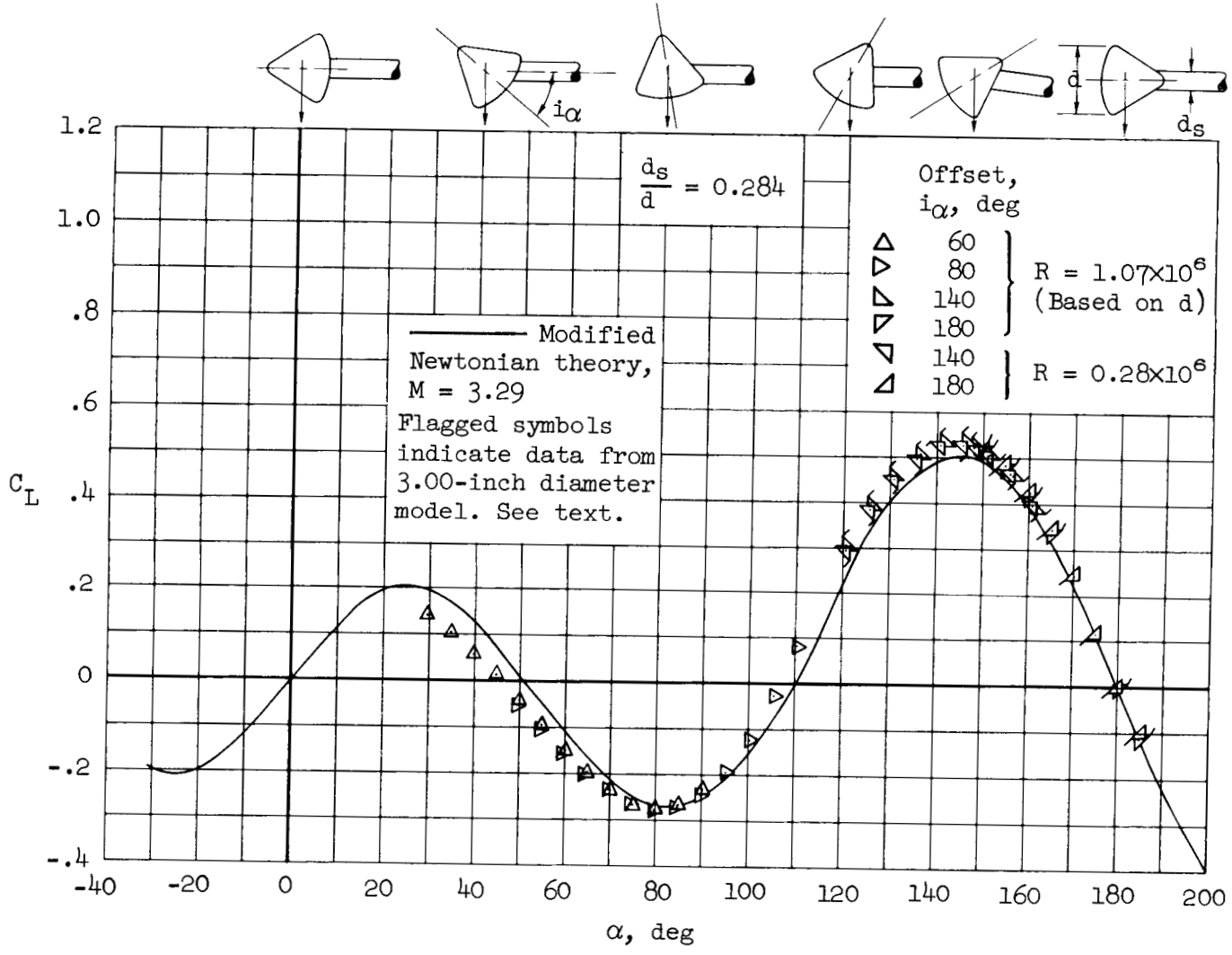

(d) C_L versus α

Figure 5.- Continued.

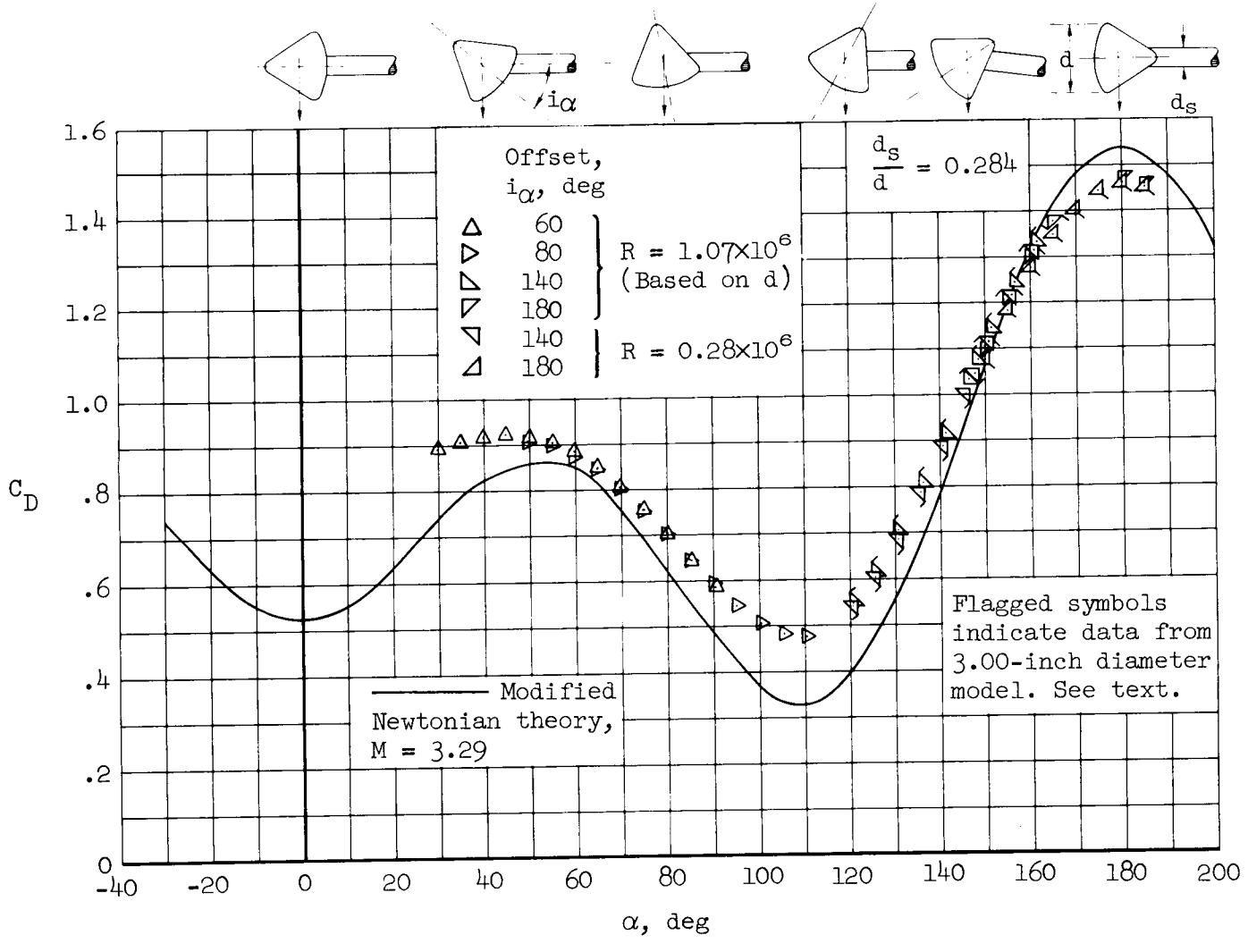

(e) C_D versus α

Figure 5.- Continued.

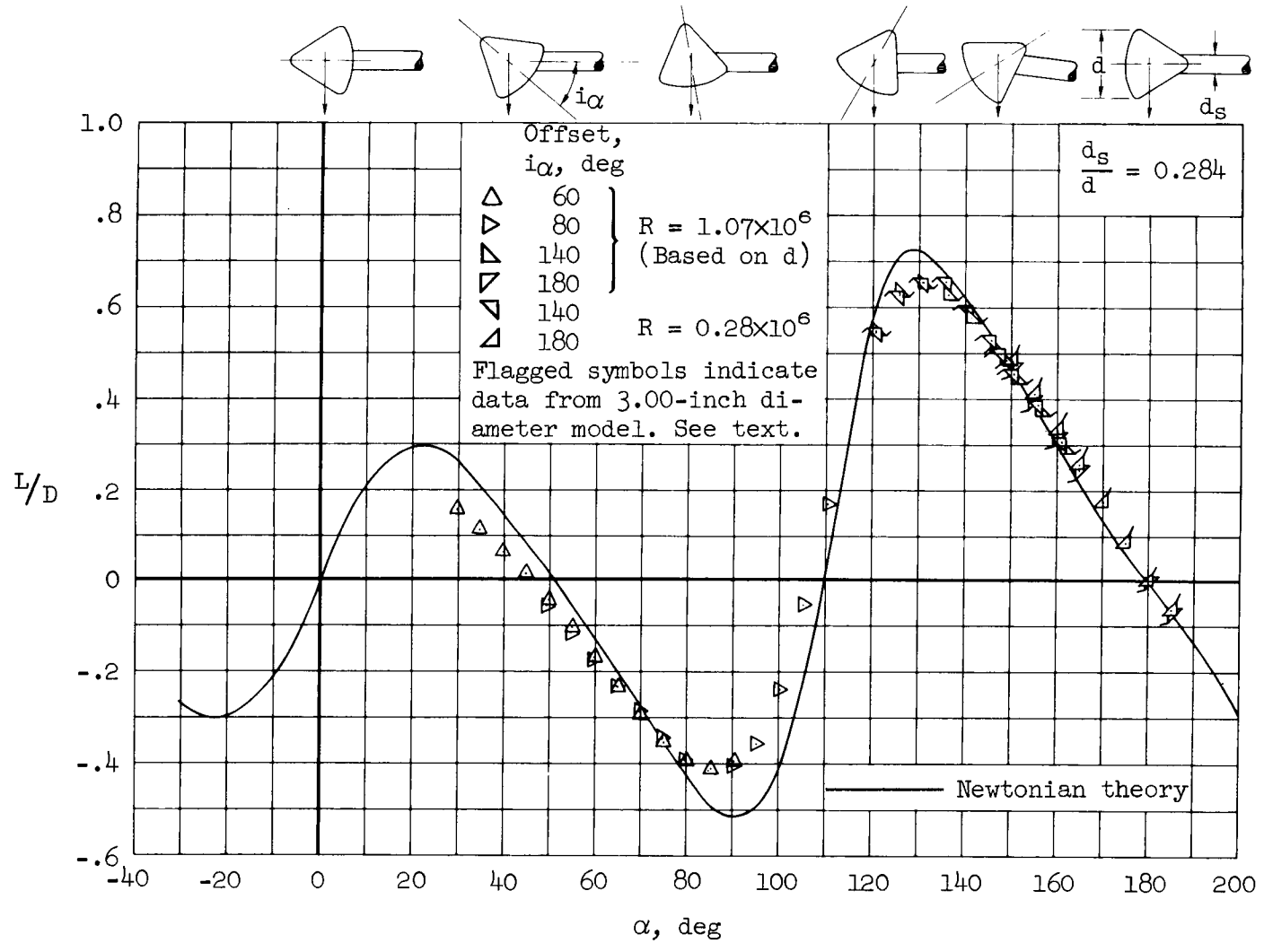

(f) L/D versus α

Figure 5.- Continued.

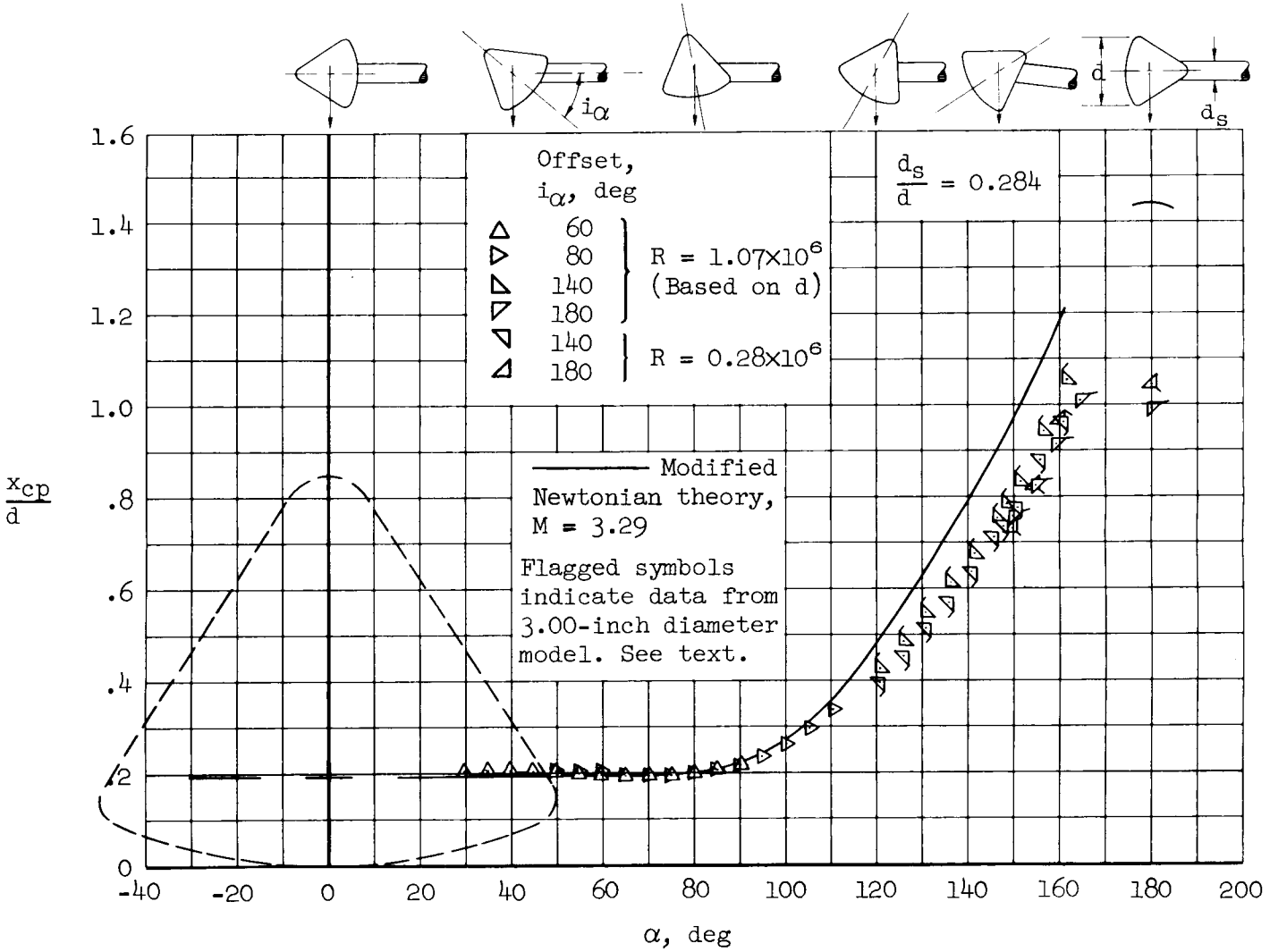

(g) $\frac{x_{cp}}{d}$ versus α

Figure 5.- Concluded.

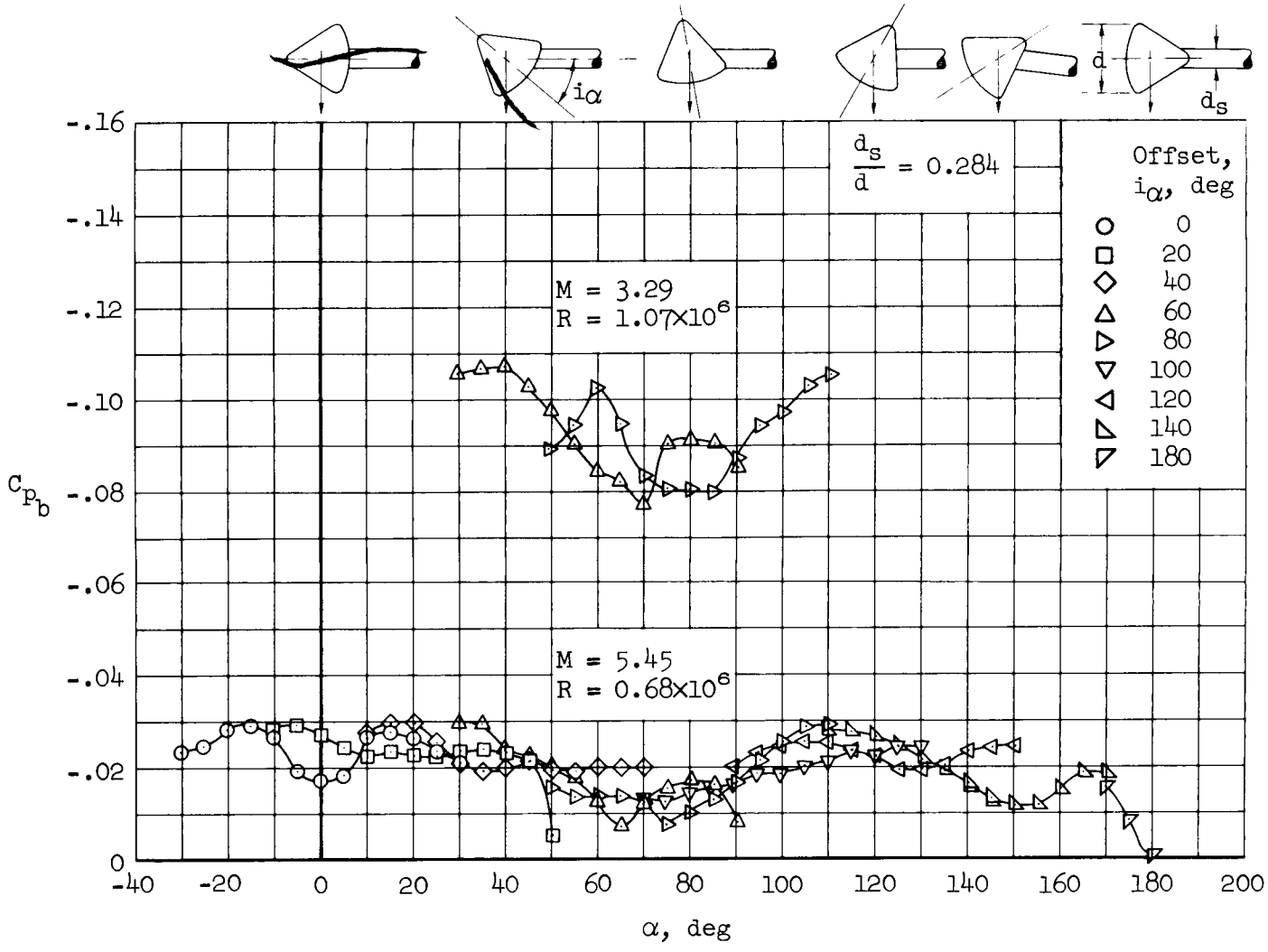

Figure 6.- Variation of balance-cavity pressure coefficient with angle of attack for Mach numbers of 5.45 and 3.29, and for Reynolds numbers of 0.68 million and 1.07 million, respectively.

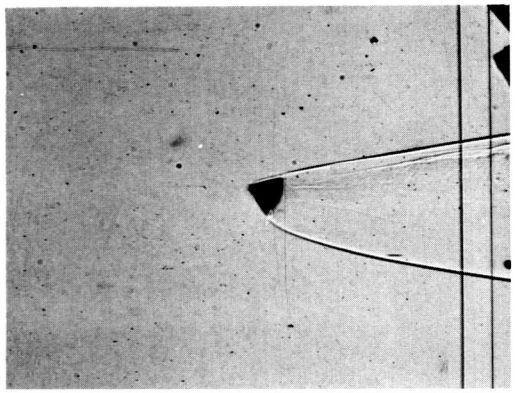

(a) M = 18.0, R = 0.52×10^6, α = 22.6°

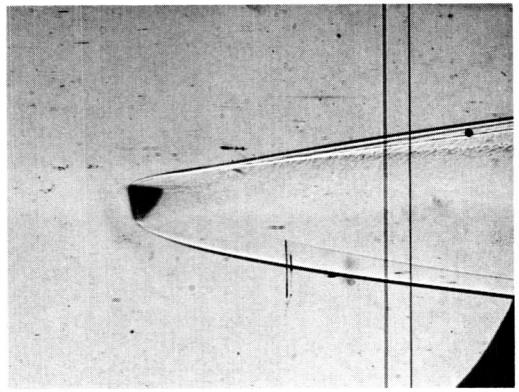

(b) M = 16.6, R = 0.72×10^6, α = 42.8°

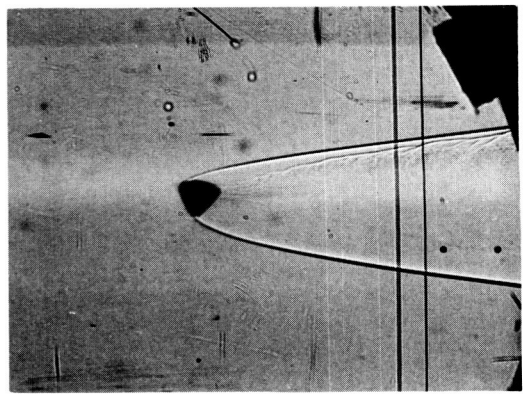

(c) M = 17.8, R = 0.51×10^6, α = -80.4°

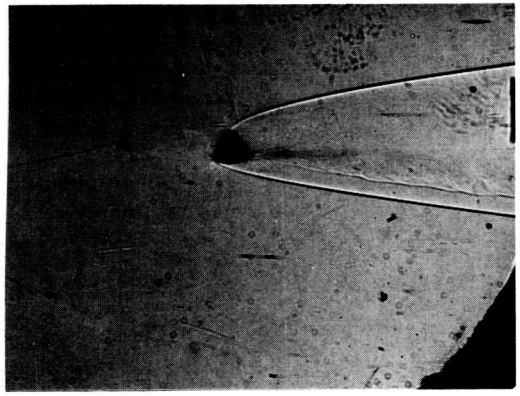

(d) M = 16.6, R = 0.48×10^6, α = 86.3°

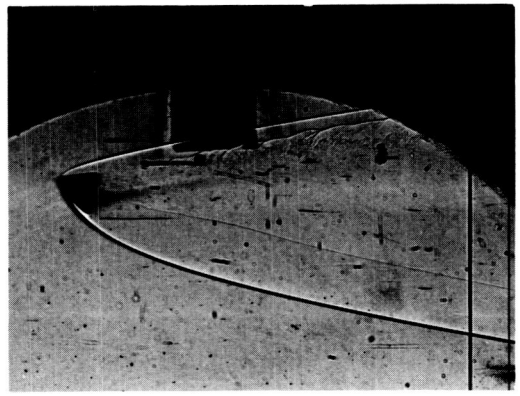

(e) M = 11.4, R = 0.65×10^6, α = 140.0°

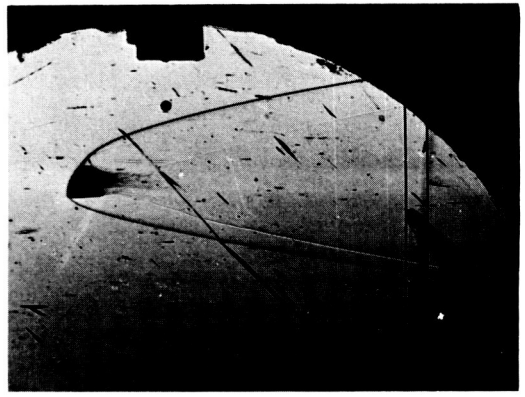

(f) M = 13.6, R = 0.77×10^6, α = -148.8°

Figure 7.- Shadowgraph pictures of approximate models of the Apollo Command Module in flight in the Ames Prototype Hypervelocity Free-Flight Facility.

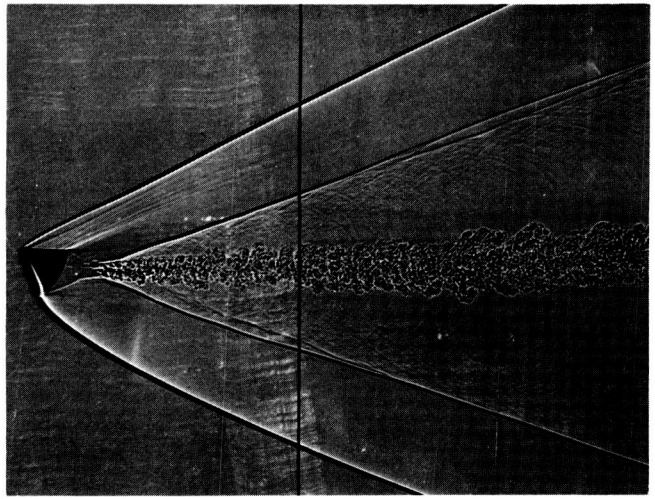

(a) M = 4.0, R = 0.58×10^6, α = 33.1°

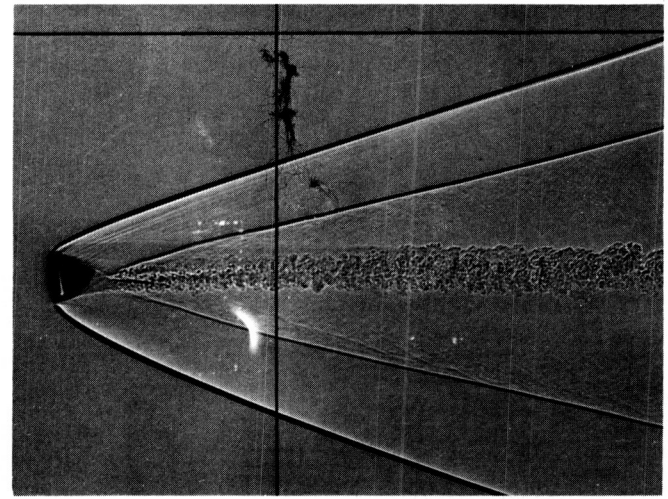

(b) M = 3.6, R = 0.52×10^6, α = 54.9°

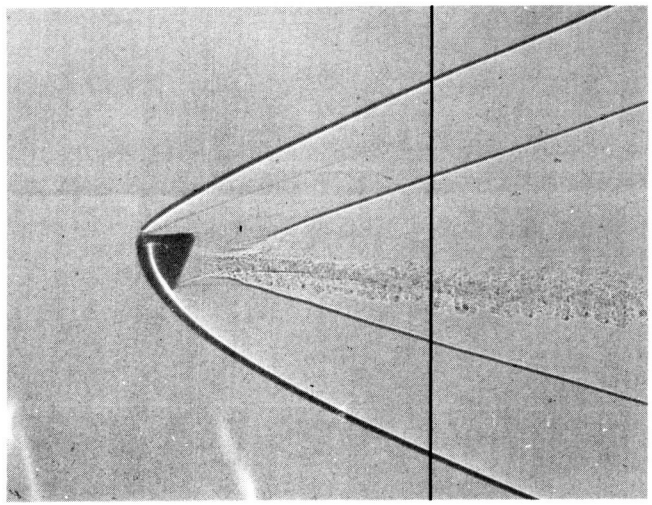

(c) M = 3.3, R = 0.58×10^6, α = 144.5°

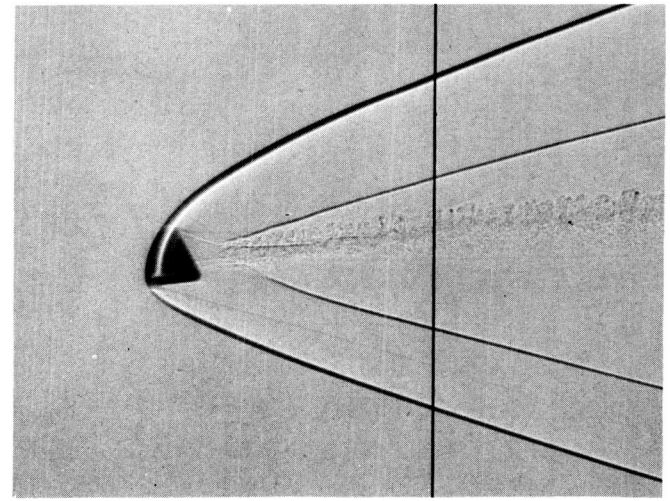

(d) M = 3.7, R = 0.58×10^6, α = -152.5°

Figure 8.- Shadowgraph pictures of approximate models of the Apollo Command Module and Mercury capsule in flight in the Ames Pressure Ballistic Range

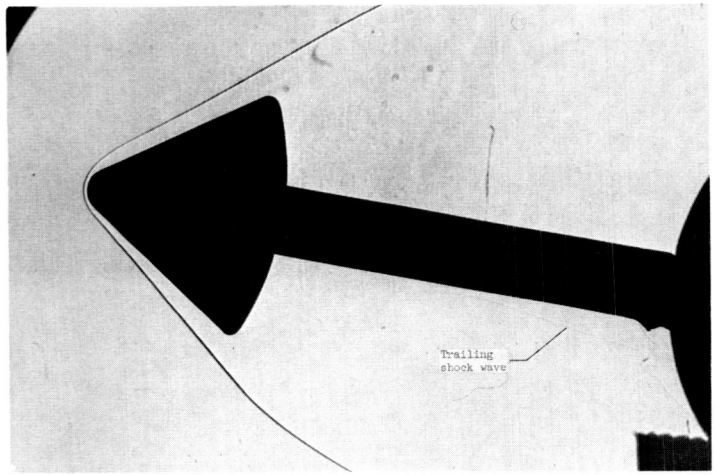

$\alpha = -10^{\circ}$, $\alpha_s = -10^{\circ}$

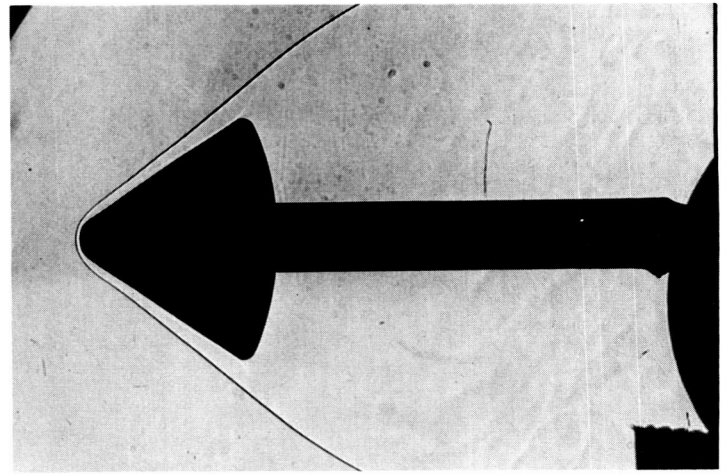

$\alpha = 0^{\circ}$, $\alpha_s = 0^{\circ}$

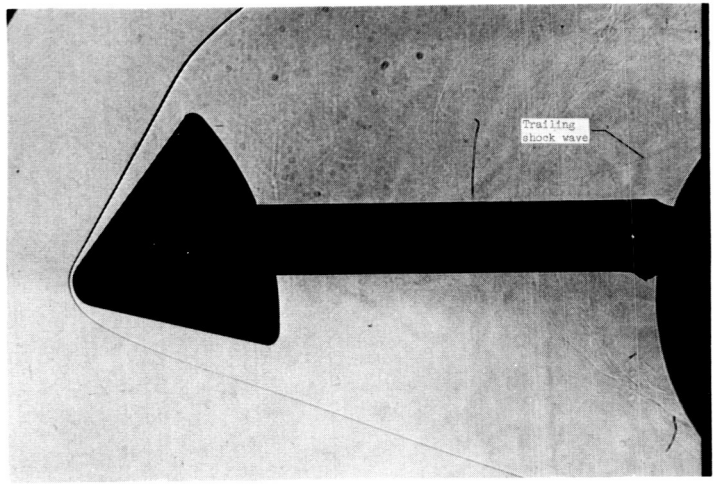

$\alpha = 20^{\circ}$, $\alpha_s = 0^{\circ}$

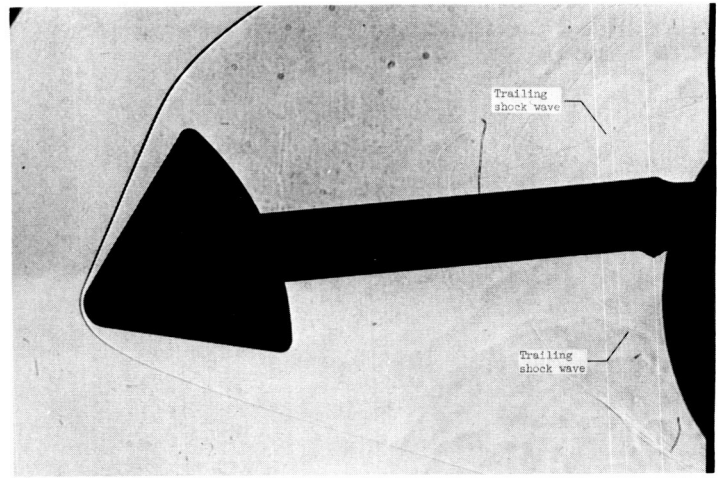

$\alpha = 25^{\circ}$, $\alpha_s = 5^{\circ}$

(a) $\alpha = -10^{\circ}$ to 25°

Figure 9.- Representative shadowgraphs of the Apollo Command Module at several angles of attack for a Mach number of 5.45 and Reynolds number of 0.68 million. Model inverted.

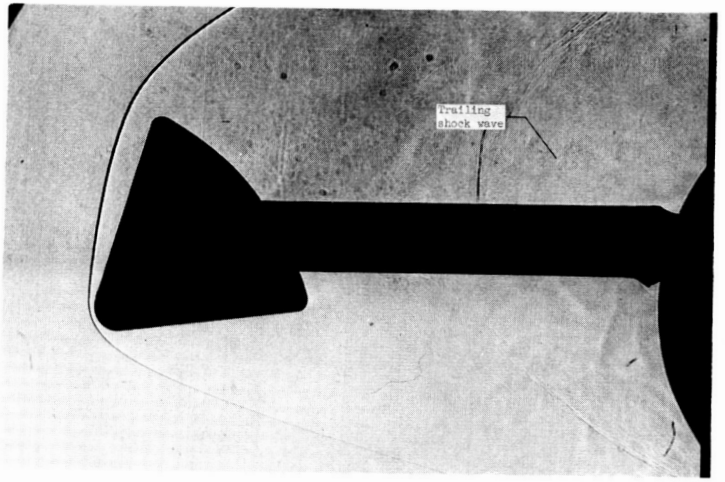

$\alpha = 40^{\circ}$, $\alpha_s = 0^{\circ}$

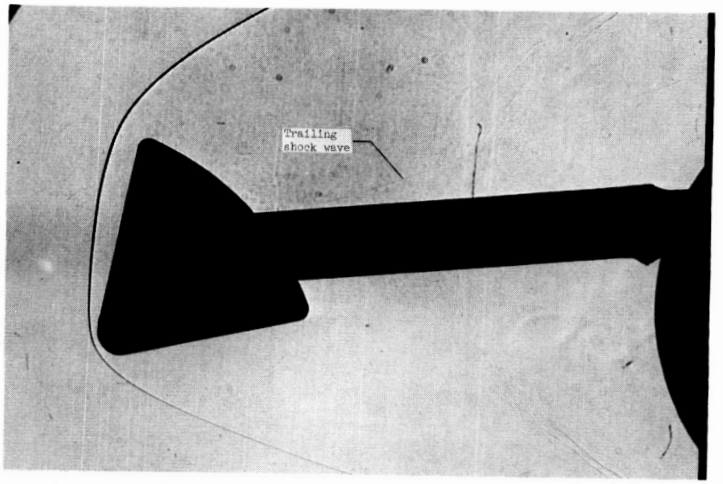

$\alpha = 45^{\circ}$, $\alpha_s = 5^{\circ}$

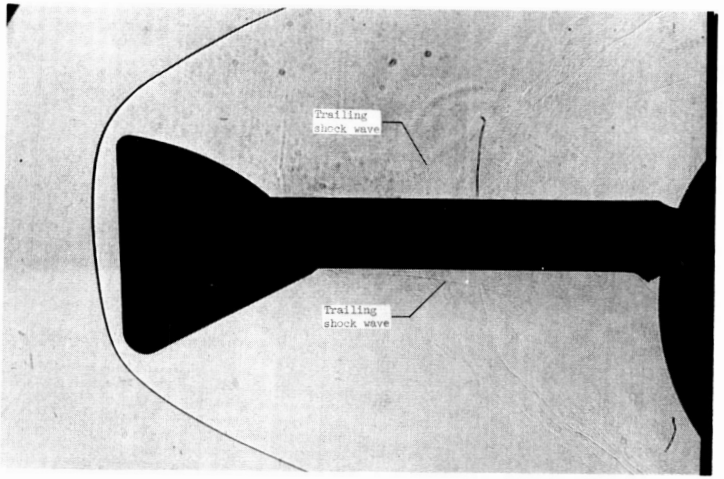

$\alpha = 60^{\circ}$, $\alpha_s = 0^{\circ}$

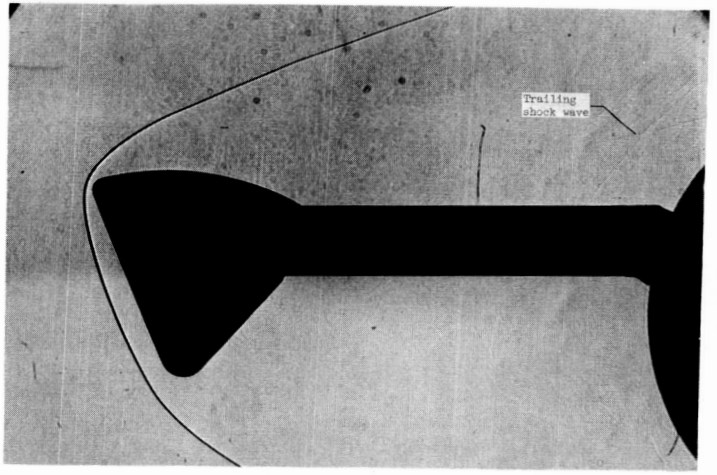

$\alpha = 80^{\circ}$, $\alpha_s = 0^{\circ}$

(b) $\alpha = 40^{\circ}$ to 80°

Figure 9.- Continued.

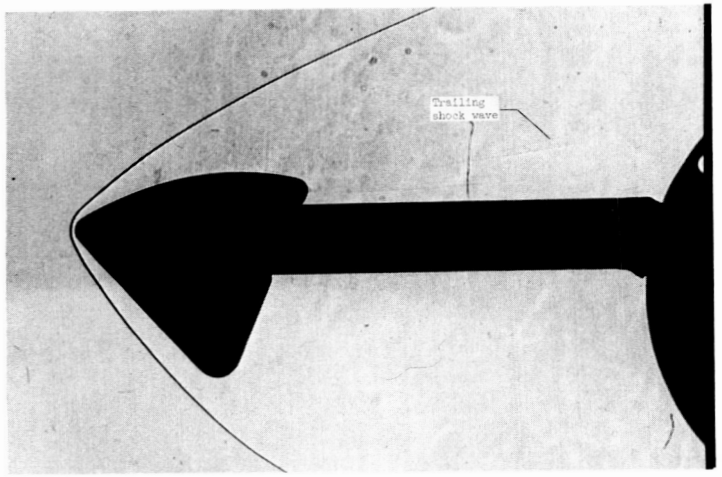

$\alpha = 100^{\circ}$, $\alpha_s = 0^{\circ}$

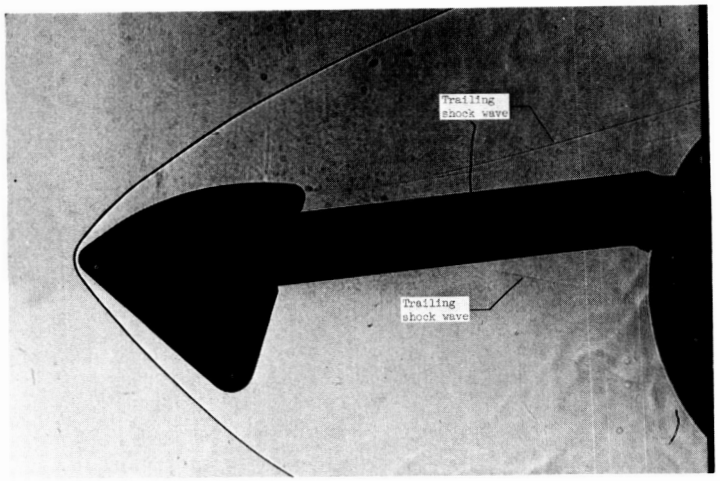

$\alpha = 105^{\circ}$, $\alpha_s = 5^{\circ}$

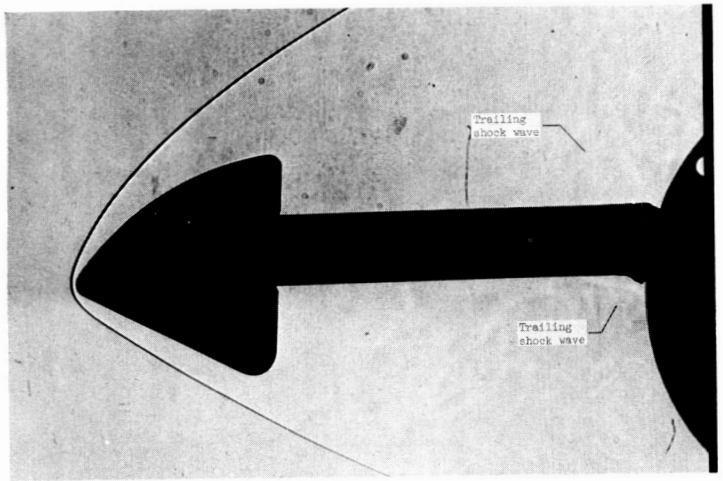

$\alpha = 120^{\circ}$, $\alpha_s = 0^{\circ}$

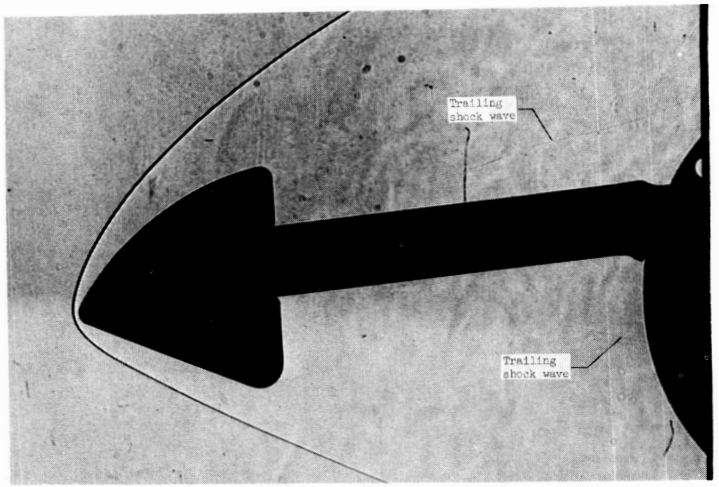

$\alpha = 125^{\circ}$, $\alpha_s = 5^{\circ}$

(c) $\alpha = 100^{\circ}$ to 125°

Figure 9.- Continued.

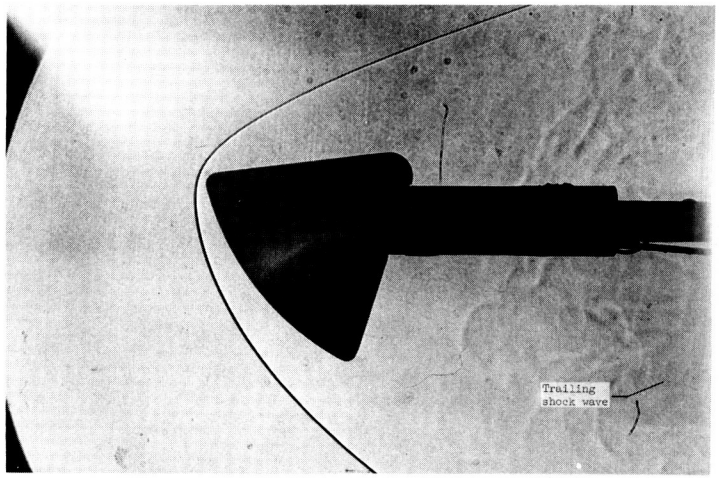

$\alpha = 140^\circ$, $\alpha_s = 0^\circ$

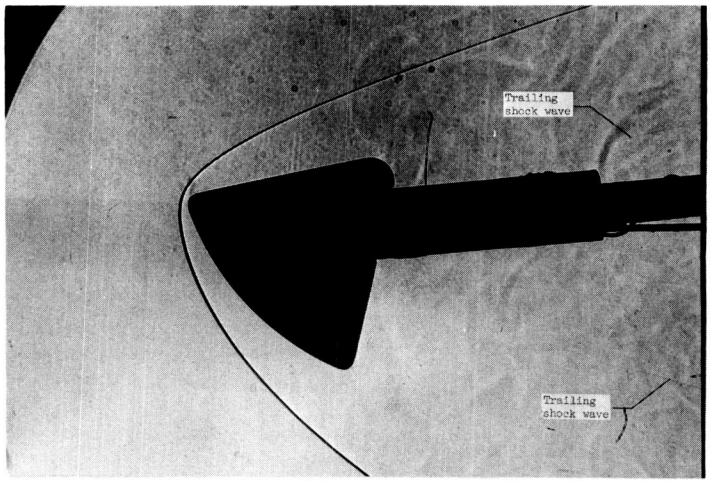

$\alpha = 145^\circ$, $\alpha_s = 5^\circ$

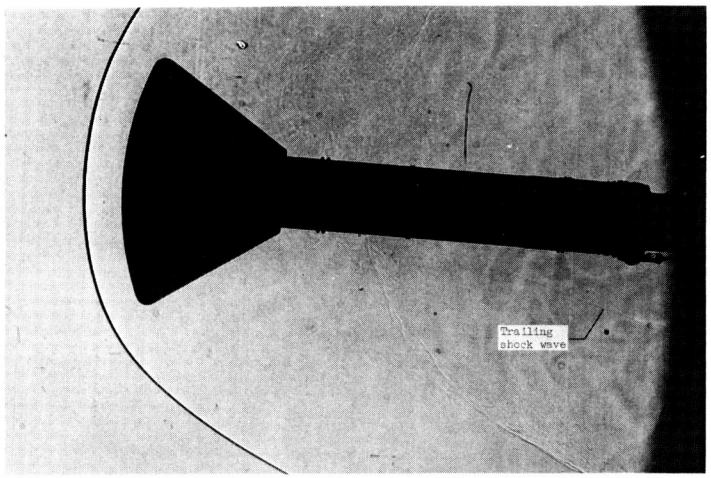

$\alpha = 175^\circ$, $\alpha_s = -5^\circ$

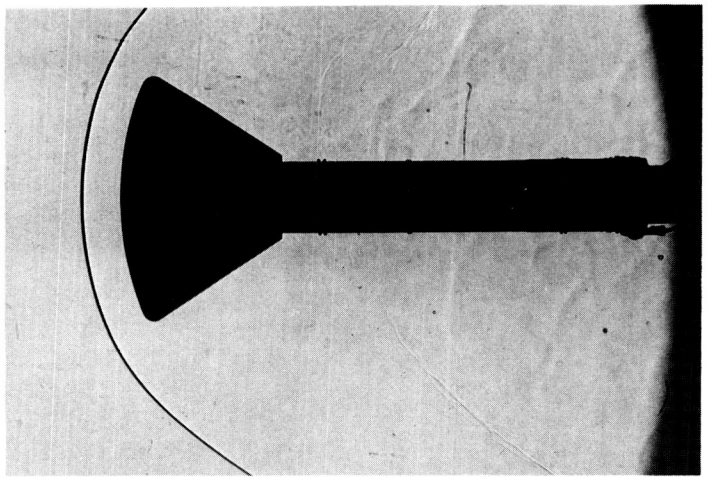

$\alpha = 180^\circ$, $\alpha_s = 0^\circ$

(d) $\alpha = 140^\circ$ to 180°

Figure 9.- Concluded.

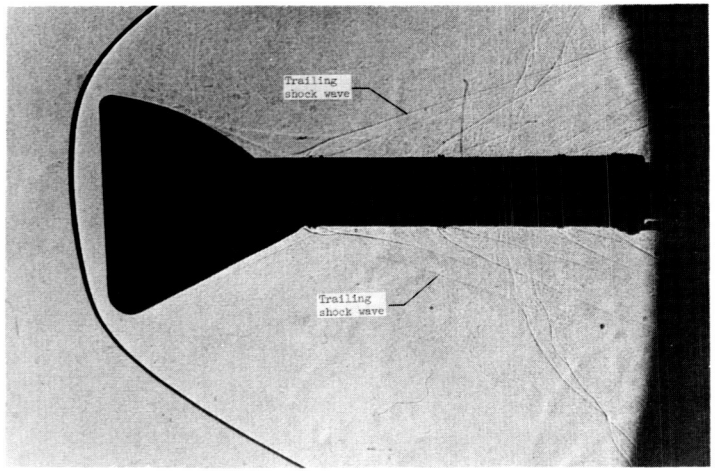

$\alpha = 60^\circ$, $\alpha_s = 0^\circ$

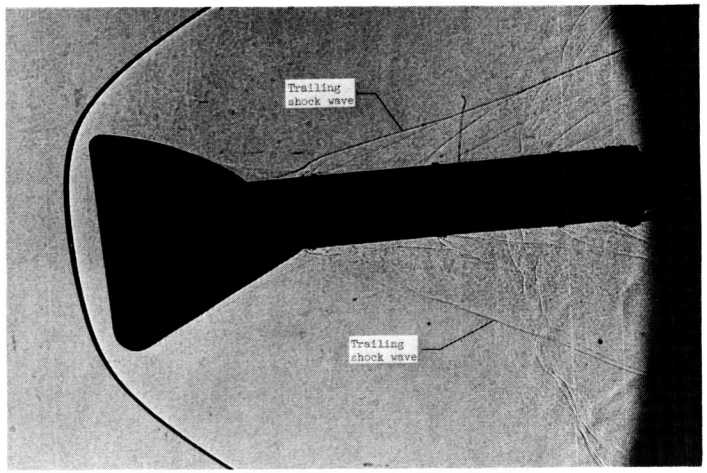

$\alpha = 65^\circ$, $\alpha_s = 5^\circ$

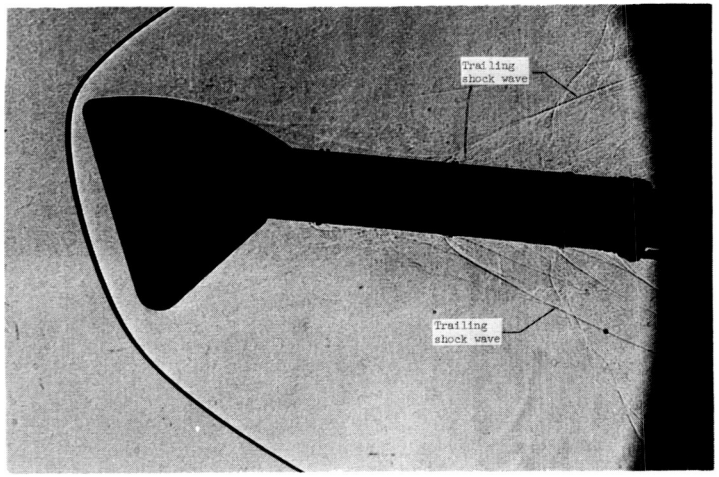

$\alpha = 75^\circ$, $\alpha_s = -5^\circ$

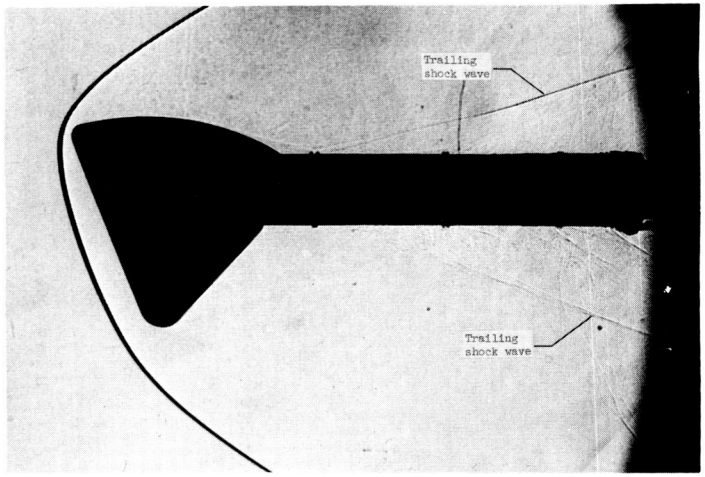

$\alpha = 80^\circ$, $\alpha_s = 0^\circ$

(a) $\alpha = 60^\circ$ to 80°, $R = 1.07 \times 10^6$

Figure 10.- Representative shadowgraphs of the Apollo Command Module at several angles of attack for a Mach number of 3.29. Model inverted.

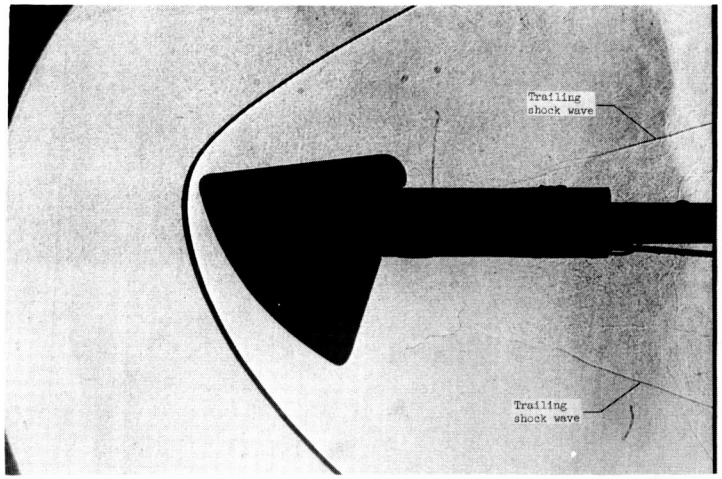

$\alpha = 140^{\circ}$, $\alpha_s = 0^{\circ}$, $R = 1.07 \times 10^6$

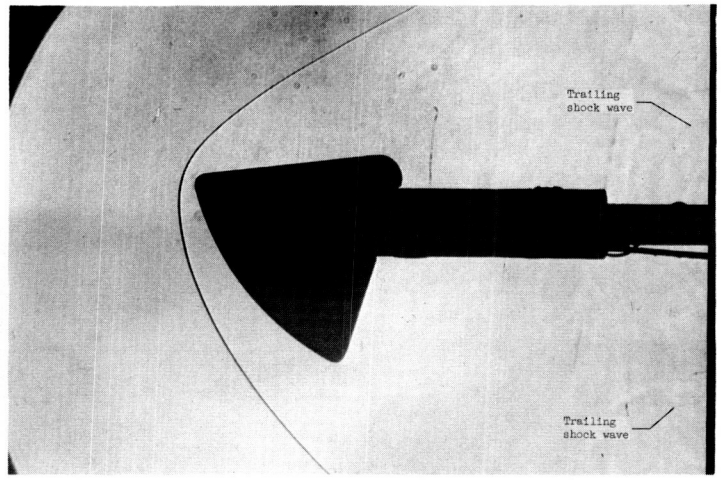

$\alpha = 140^{\circ}$, $\alpha_s = 0^{\circ}$, $R = 0.28 \times 10^6$

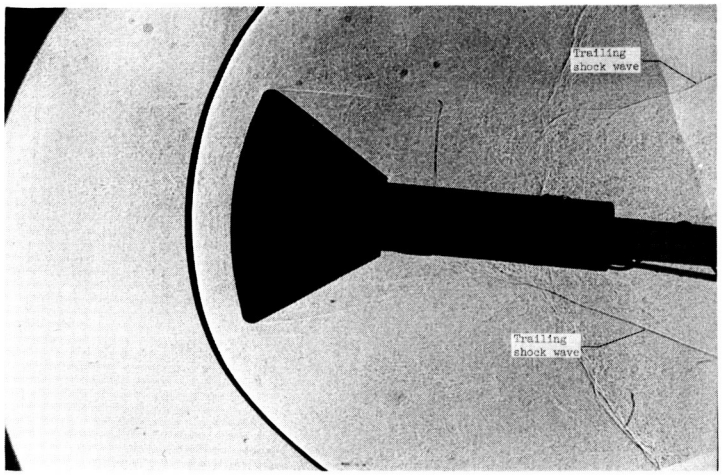

$\alpha = 175^{\circ}$, $\alpha_s = -5^{\circ}$, $R = 1.07 \times 10^6$

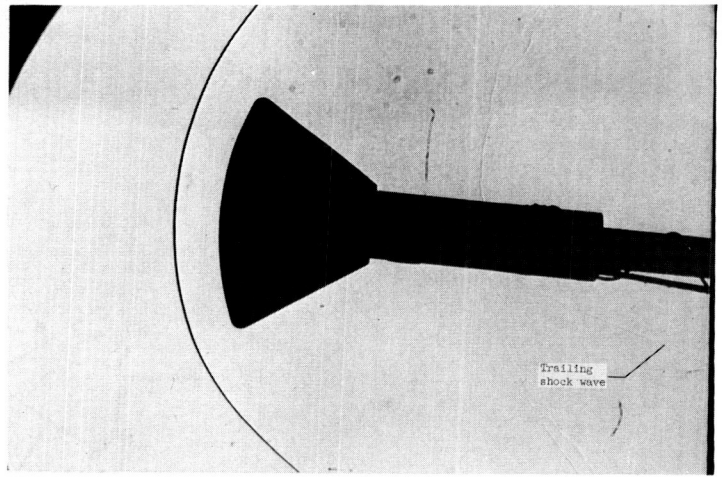

$\alpha = 175^{\circ}$, $\alpha_s = -5^{\circ}$, $R = 0.28 \times 10^6$

(b) $\alpha = 140^{\circ}$ and 175°

Figure 10.- Concluded.

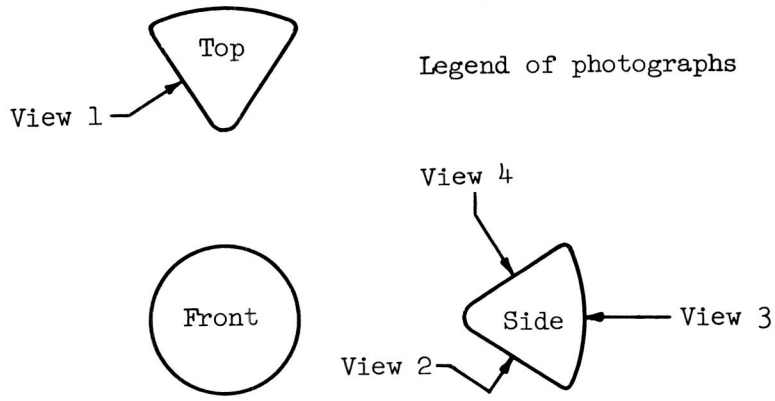

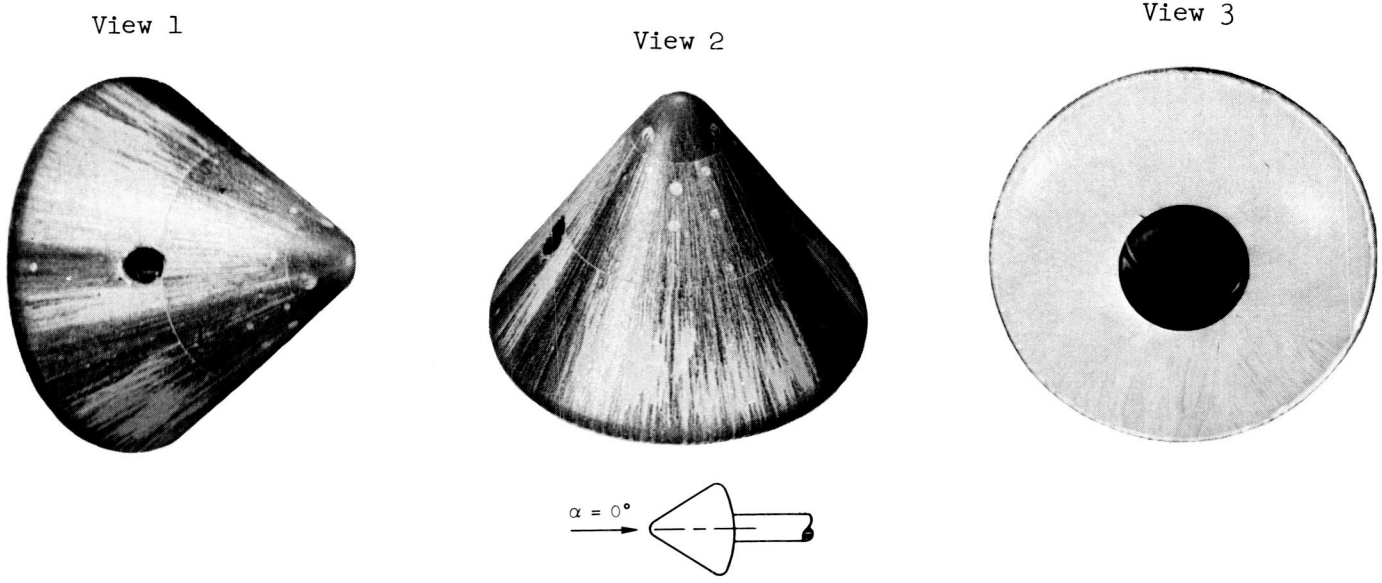

(a) $\alpha = 0$

Figure 11.- Photographs of the oil-flow patterns on the Apollo Command Module at several angles of attack for a Mach number of 3.29; $R = 0.75 \times 10^6$

View 1 View 2 View 3 View 4

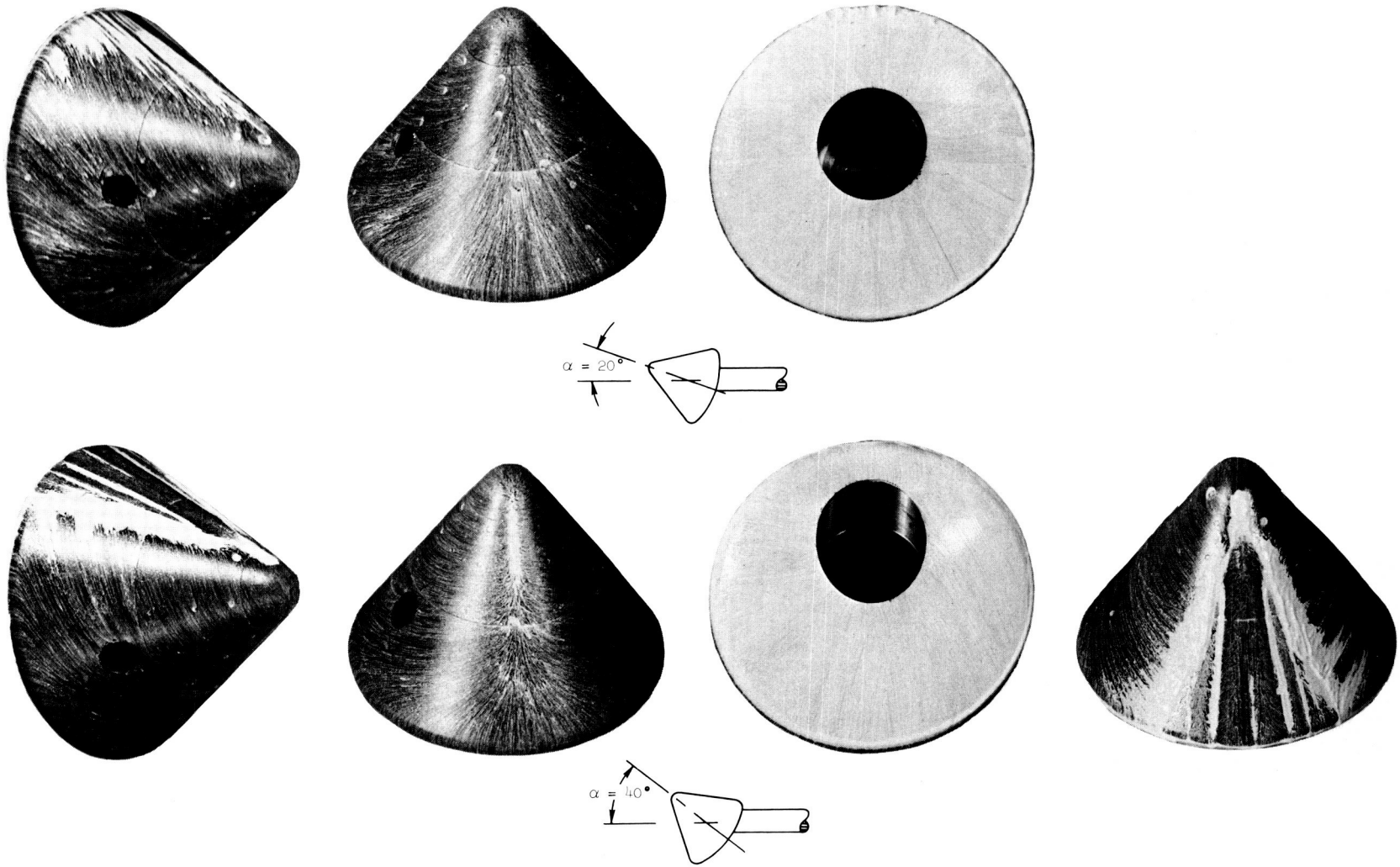

(b) $\alpha = 20^{\circ}$ and 40°

Figure 11.- Continued.

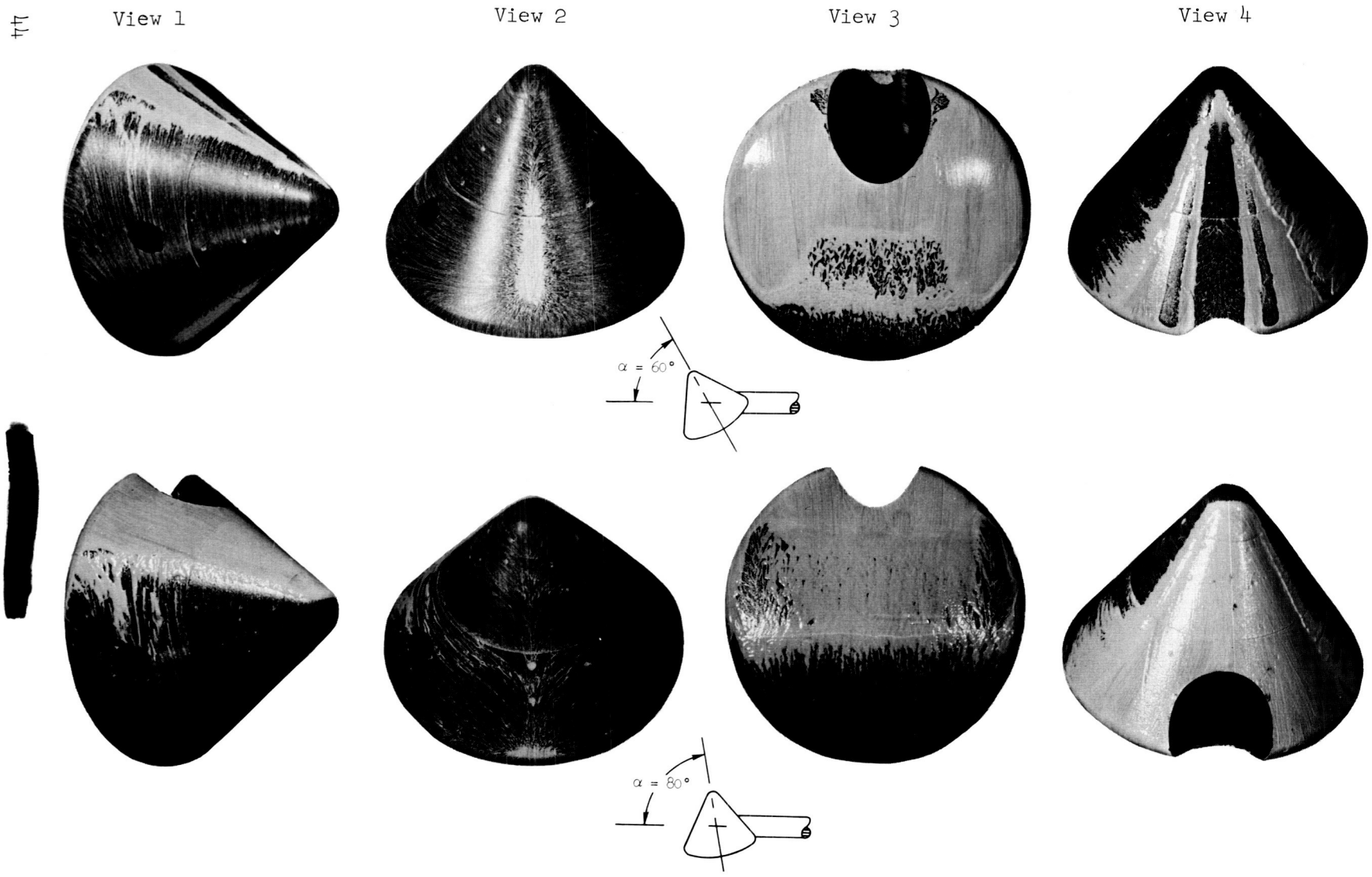

(c) $\alpha = 60^{\circ}$ and 80°

Figure 11.- Continued.

View 1 View 2 View 3

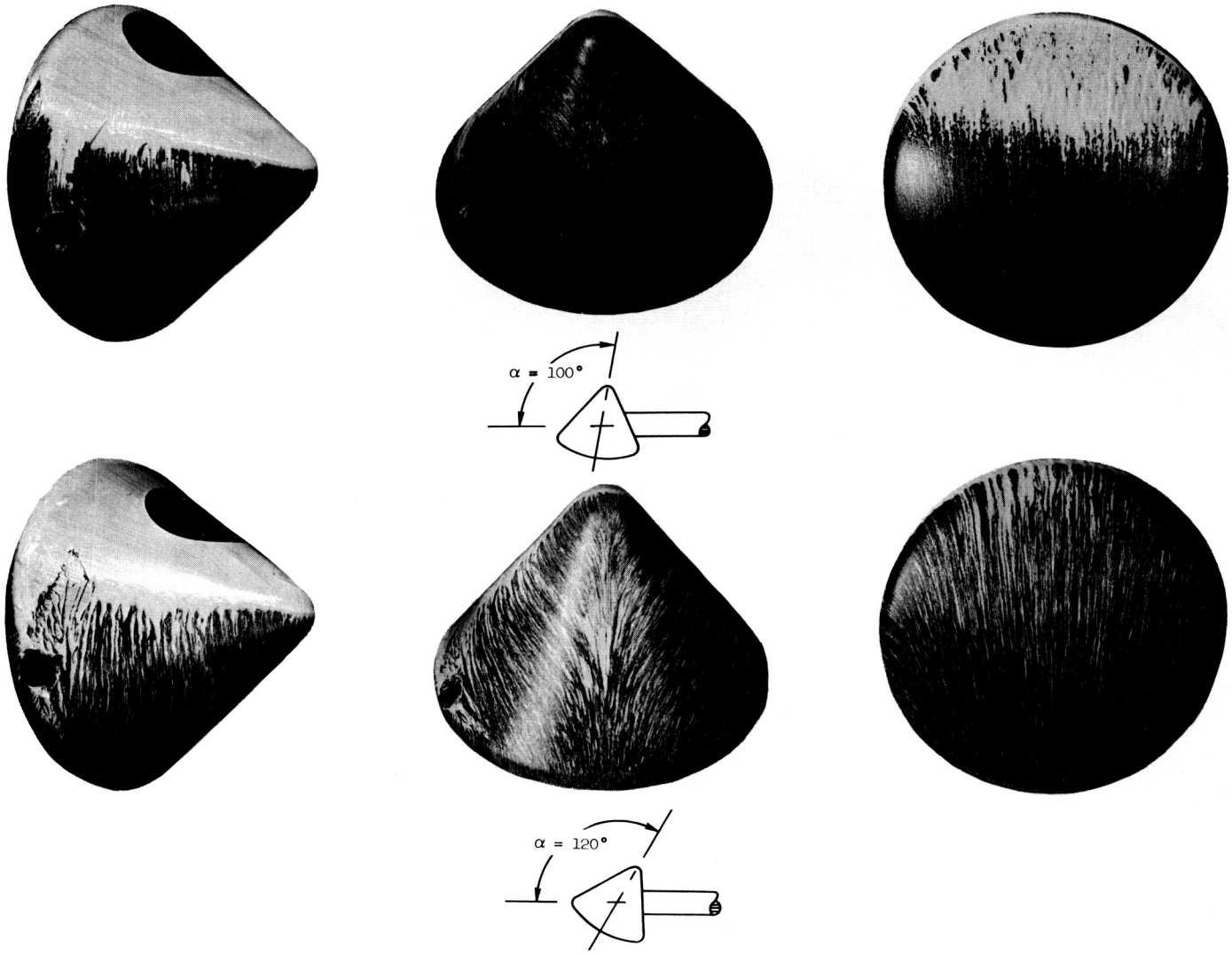

(d) $\alpha = 100^{\circ}$ and 120°

Figure 11.- Continued.

View 1 View 2 View 3

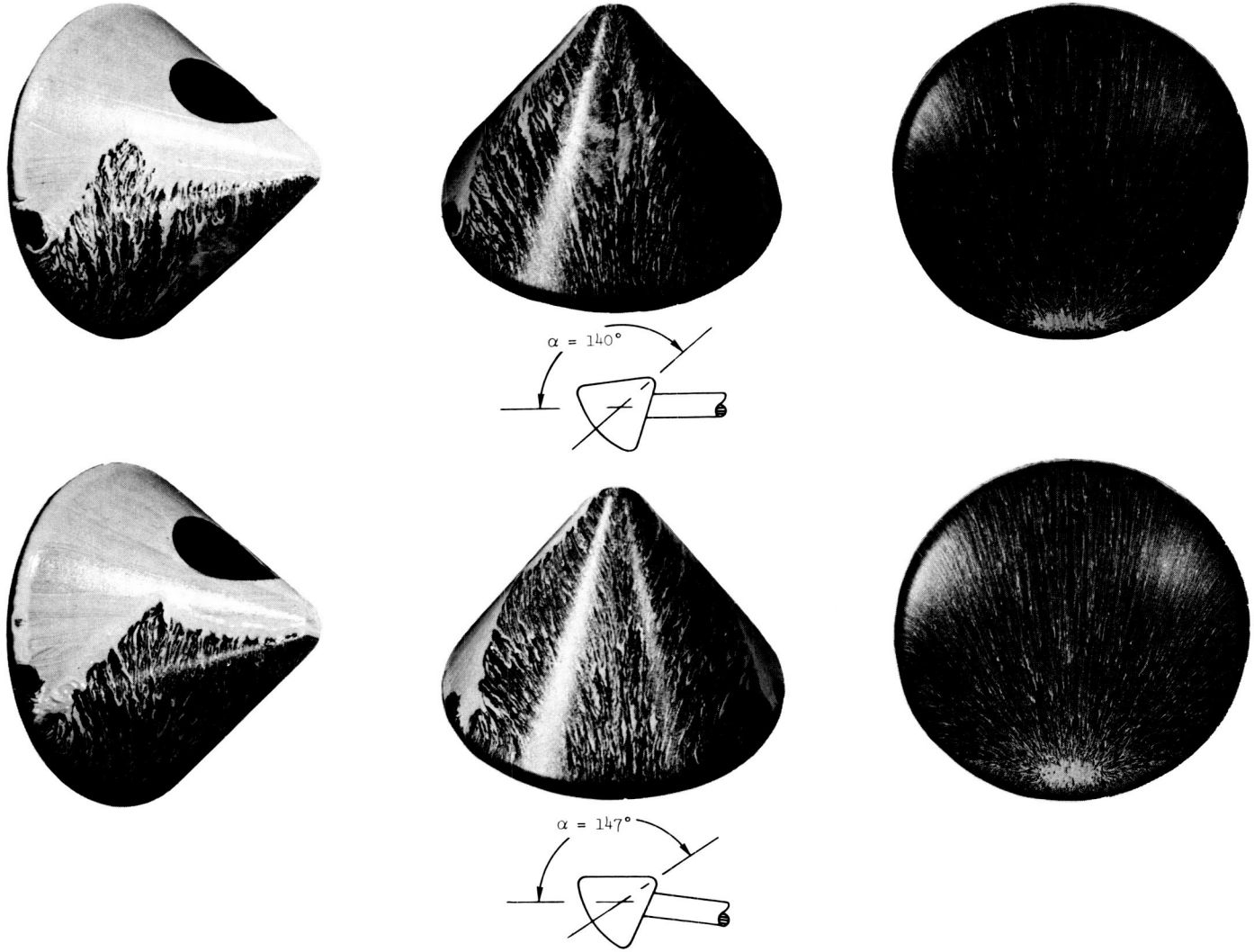

(e) $\alpha = 140^{\circ}$ and 147°

Figure 11.- Continued.

View 1

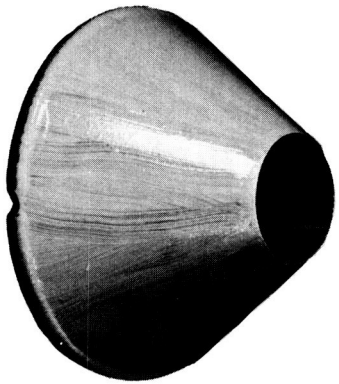

View 2

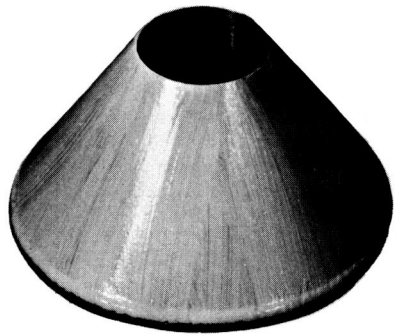

View 3

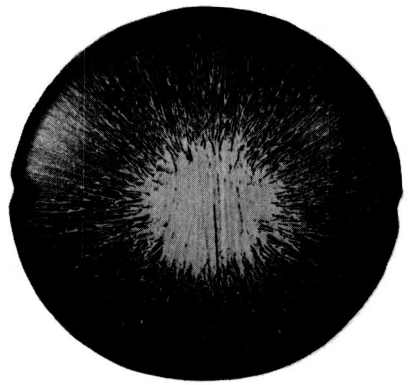

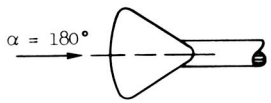

(f) $\alpha = 180^{\circ}$

Figure 11.- Concluded.

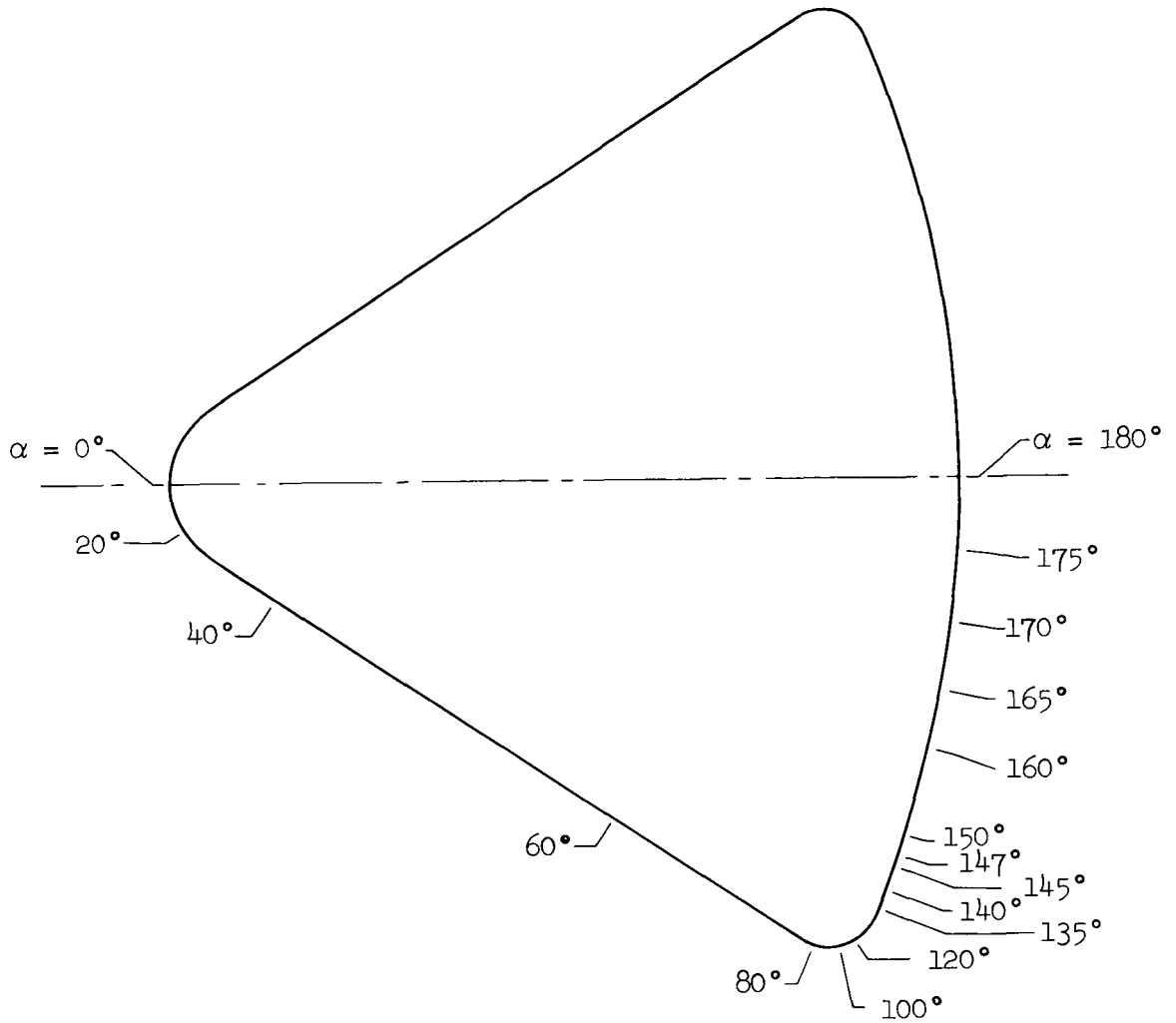

(a) Location on the profile.

Figure 12.- Variation with angle of attack of the stagnation-point location on the Apollo Command Module; M = 3.29, R = 0.75×10^6.

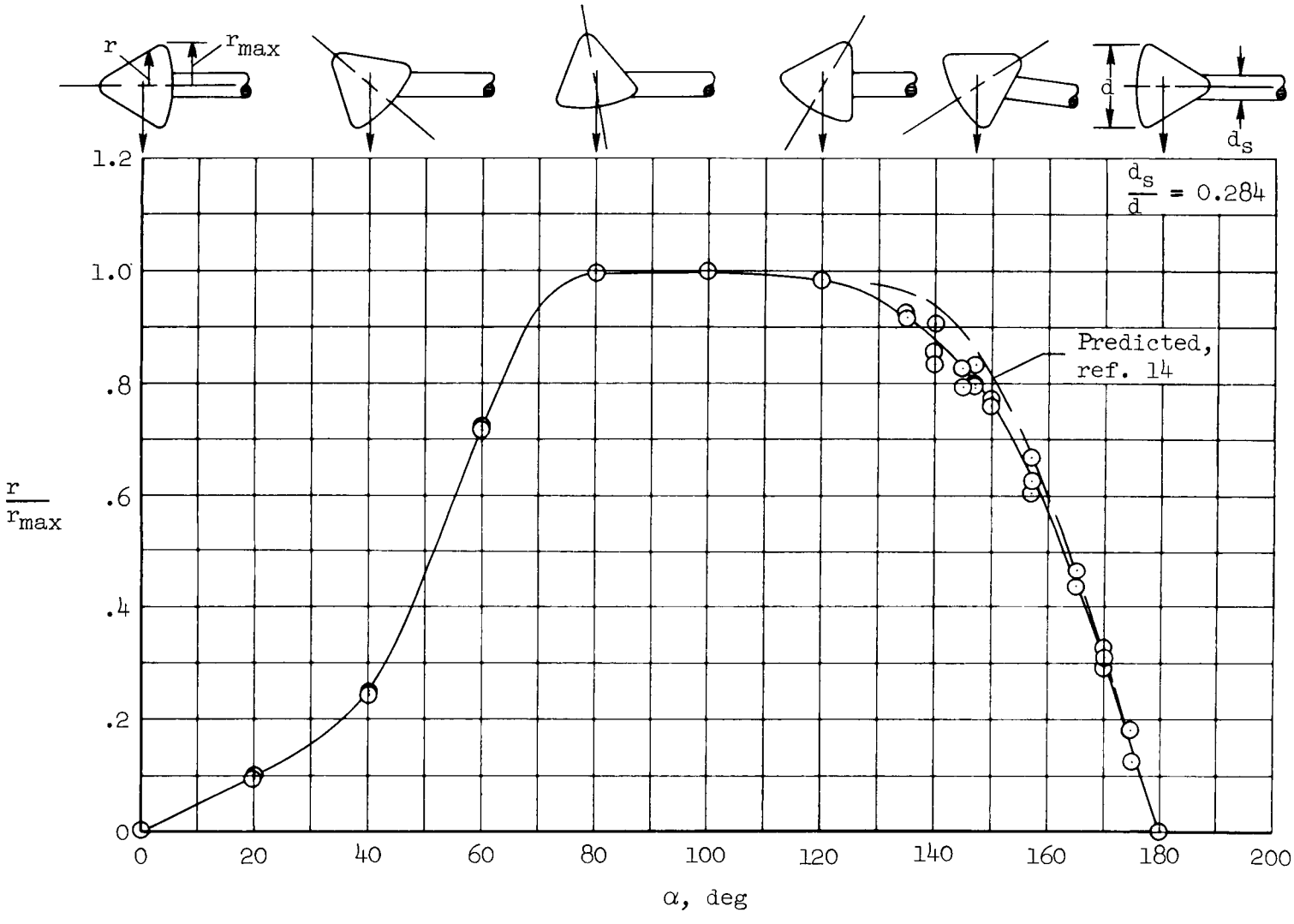

(b) Radial location.

Figure 12.- Concluded.

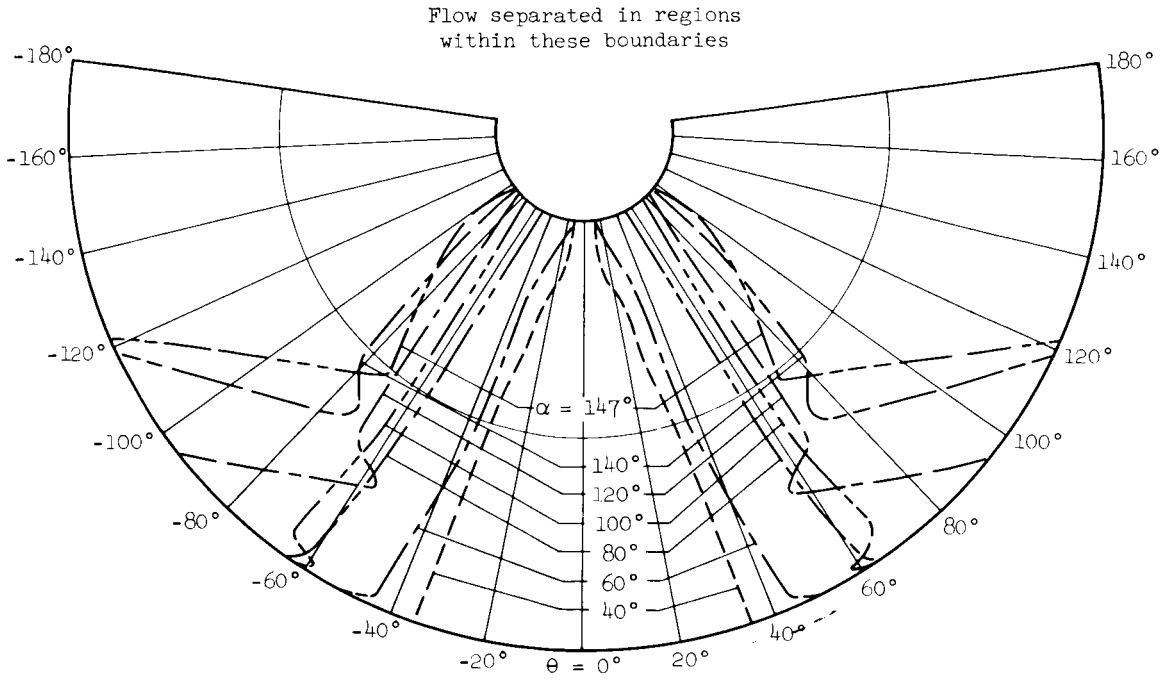

Developed surface of conical portion.

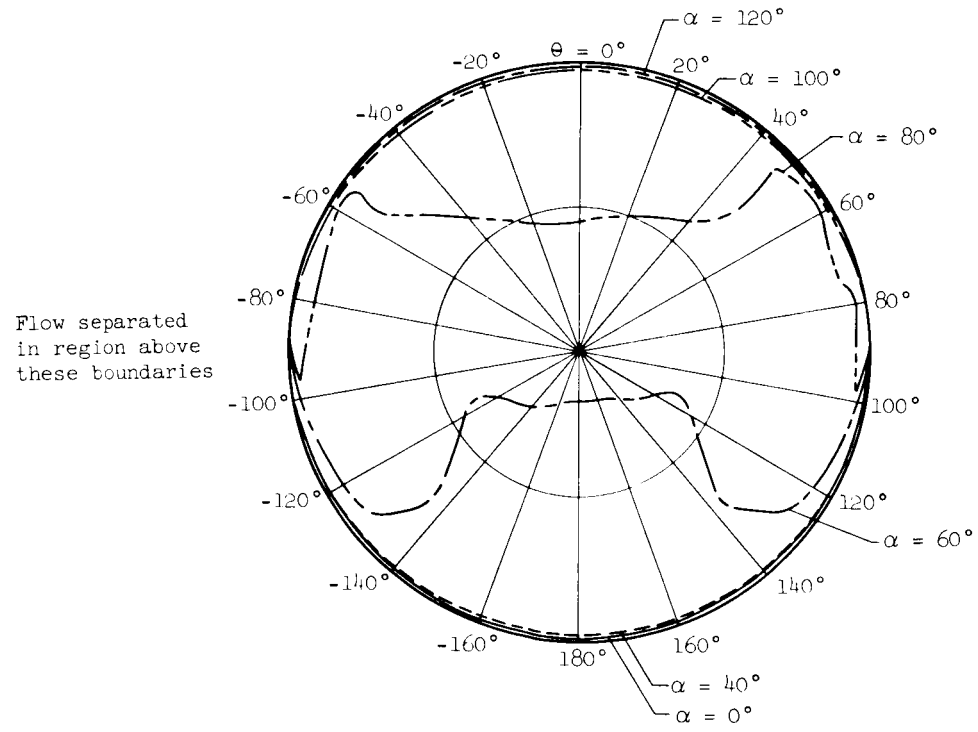

Projected view of spherical portion.

Figure 13.- Boundaries of separation on the surface of the conical and spherical portions of the Apollo Command Module at various angles of attack for a Mach number of 3.29; $R = 0.75 \times 10^6$.

NASA-Langley, 1965 A-978